Universitat de les Illes Balears

ÉCOLE NATIONALE de la MÉTÉOROLOGIE
METEO FRANCE ENM

End of studies training report n° 1140

Convective initiation over the data-void Mediterranean Sea, a challenge for mesoscale numerical models: The severe thunderstorm of 4^{th} October 2007 in Mallorca

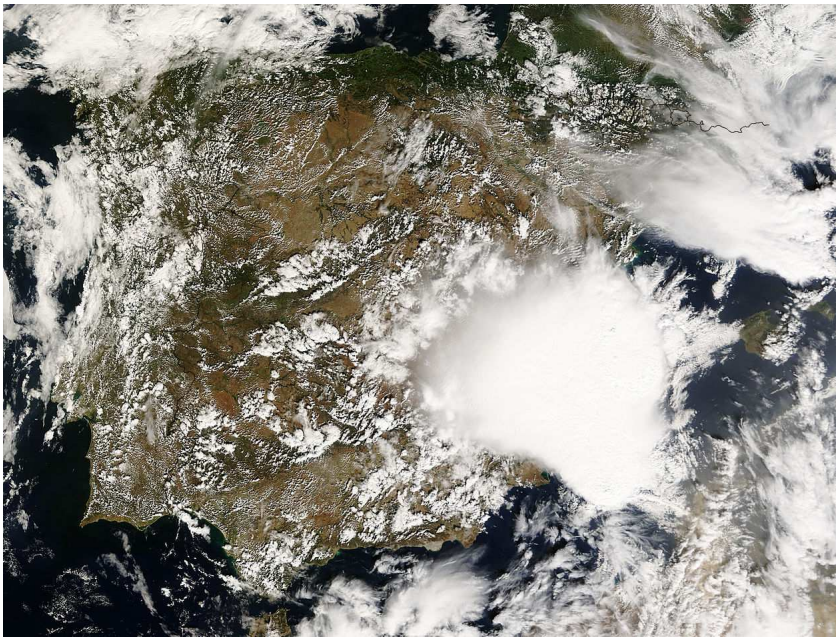

COHUET Jean-Baptiste

End of studies training
realized at the Grup de Meteorologia of the Universitat de les Illes Balears,
supervised by Romualdo Romero, Víctor Homar and Véronique Ducrocq,
from 19^{th} January to 19^{th} June 2009
Promotion of ENM engineers students 2006-2009

2009

Acknowledgments

This present study is the result of a close collaboration between the Universitat de les Illes Balears and the CNRM of Météo France. I want to acknowledge all the people in both research teams who have made this work possible.

First of all, I gratefully acknowledge my duet of complementary tutors, Romualdo Romero and Víctor Homar for their hearty welcome in the group. I have particularly liked their skills on numerous meteorological fields, their kindness, and their availability during these five months. I have hugely appreciated their corrections to improve the English of the manuscript. More precisely, I have greatly benefited from exchanges with Romualdo to carry out this project, and I am thankful for its clear teachings. I deeply thank Víctor for its relevant ideas, as well on meteorological topics as in computing to deal with the three models. I have enjoyed his optimism to overcome trials all along my training.

In addition, I acknowledge Véronique Ducrocq who allowed me to do this research project. I am grateful for her tutoring during the first step of my training at the CNRM, and for the interest she had on my work during the second part. I also acknowledge Christine Lac for the follow-up of my training, and for her contributions to improve the quality of the report thanks to her pertinent suggestions.

I have appreciated conversations with Climent Ramis and I thank him for his interesting ideas and for his previous work on the case that I have studied. I also acknowledge Maria Antonia Jimenez for her advices on planetary boundary layer topics.

Thanks are also due to Juan Escobar from the Laboratoire d'Aérologie whose help was essential to succeed in running Méso-NH at the UIB. Besides, I acknowledge Gaëlle Tanguy for her very usefull remote assistance on Méso-NH and for the numerous data transfer she made. In addition, I thank Pierrick Cébron for important data that he provided to me.

I am thankful for Regina Guilabert, Jose Arrecio and Laurent Labatut for their software assistance as well in Palma as in Toulouse.

At least, I thank all the staff of both research teams, the Grup de Meteorología and MICADO, for their welcome and their advices during my training period.

Short abstract

The Mediterranean basin is regularly affected by severe weather associated with deep convection. Even if they are usually tied to coastal orography, some severe thunderstorms develop and mature over the sea. A good and recent example is the severe thunderstorm that crossed the island of Mallorca in the afternoon of 4^{th} October 2007. Generated early in the morning offshore of Murcia, this storm organized progressively into a squall line structure with a northeastwards movement. Arriving in Palma city, this squall line was accompanied by severe gusts, heavy rain and several tornadoes, leading to significant damages in the southwestern part of the island and eventually to one fatality.

The triggering and evolution of convection in these maritime events depend on both synoptic and mesoscale features. Representing such interaction is a real challenge for numerical models used in weather forcasting. The aim of this study is to determine the most influential factors involved in the initiation and evolution of the damaging squall line, thanks to several combinations of numerical models (Méso-NH, WRF and MM5) with different initial and boundary conditions. This ensemble of simulations has allowed to gain insight on which mechanisms are the most relevant to obtain an accurate spatiotemporal representation of the squall line. In addition, synthetically generated observations allow to confirm the crucial role of a convergence line offshore of Murcia in the triggering and evolution of the squall line. Furthermore, a high sensitivity of convective initiation to planetary boundary schemes was pointed out and the circulation induced by the Atlas mountain range was shown to affect the convective triggering location. Finally, the lack of observations over the Mediterranean sea hampers the simulations accuracy due to the absence of important structures in the initial and boundary conditions. Nevertheless, the best simulations show a very realistic representation of the squall line, including mesovortices ahead of the gust front, that confirm the presence of a favourable environment for the genesis of small vortices, including tornadoes.

Résumé court

Le bassin méditerranéen est régulièrement affecté par des épisodes dévastateurs de convection profonde. Même si l'occurrence de tels phénomènes est souvent dépendante du relief du littoral, certaines puissantes cellules orageuses se développent et évoluent sur la mer. La ligne de grains qui traversa l'île de Majorque dans l'après-midi du 4 octobre 2007 en est un bon exemple récent. Après la formation d'une cellule convective tôt le matin au large de Murcia, cet orage s'est progressivement organisé en ligne de grains au fil d'un parcours maritime. En arrivant sur la ville de Palma, les puissantes rafales, les pluies diluviennes et les tornades associées ont entrainé de sérieux dégâts ainsi que la mort d'une personne.

Le déclenchement de la convection et son évolution lors de ces épisodes maritimes dépendent à la fois d'éléments d'échelle synoptique et de méso-échelle. Représenter une telle interaction est un enjeu important pour les modèles numériques de fine résolution utilisés en prévision. Le but de ce travail est d'étudier le cas du 4 Octobre 2007 en combinant plusieurs modèles numériques (Méso-NH, WRF et MM5) avec diverses conditions initiales et aux limites. Cet ensemble de simulations a permis de comprendre quels mécanismes étaient les plus importants pour obtenir une bonne représentation spatio-temporelle de la ligne de grains. De plus, l'assimilation de pseudo-observations subjectives a mis en évidence que la présence d'une ligne de convergence au large de Murcia avait un rôle important pour déclencher la convection. Par ailleurs, une grande sensibilité de l'initiation convective au schéma de couche limite employé par les modèles numériques a été découverte, et la circulation induite par le relief de l'Atlas tend à préciser la localisation de la cellule orageuse initiale. Le manque d'observations sur la Méditerranée se traduit dans certains cas par l'absence de structures importantes dans les conditions initiales et aux limites des modèles, ce qui pénalise la qualité des résultats. Néanmoins, les meilleures simulations parviennent à une modélisation très réaliste de la ligne de grains, incluant la formation de mésovortex à l'avant du courant de densité, ce qui confirme la présence d'un environnement favorable à la naissance de tornades.

Extended abstract

Mediterranean coastal regions are often affected by severe convective storms, especially during the fall when the sea is quite warm. The main part of these events are triggered by coastal orography present along the Mediterranean seashore. However, in some cases like the squall line of 4^{th} October 2007 that affected the island of Mallorca, mesoscale convective systems develop and mature over the sea. The aim of this study is to simulate this severe thunderstorm event by means of several combinations of three mesoscale numerical models with different initial and boundary conditions in order to understand the meteorological environment that sustained the triggering and evolution of such devastating squall line.

On 4^{th} October 2007 weather conditions were favourable to deep convection developments. Aloft, a cold cut off located over mainland Spain (figure 1-a) was associated with an anomaly of potential vorticity along a southerly and divergent jet streak. At low-levels, a baroclinic boundary spreading along Spanish coast (figure 1-b) and characterized by a katafront structure marked the limit of a warm and moist air mass lying over the Mediterranean sea. In this environment, a convective cell triggered offshore of Murcia (southeast Spain) early in the morning (figure 2-a). After a quasi-stationary stage in which the thunderstorm presented a V-shaped structure, it organized progressively into a squall line with a northeastwards movement (figure 2-b). Arriving in Palma city, this squall line was accompanied by severe gusts, heavy rain and several F2-F3 tornadoes on Fujita scale, leading to significant damages in the southwestern part of the island and eventually to one fatality.

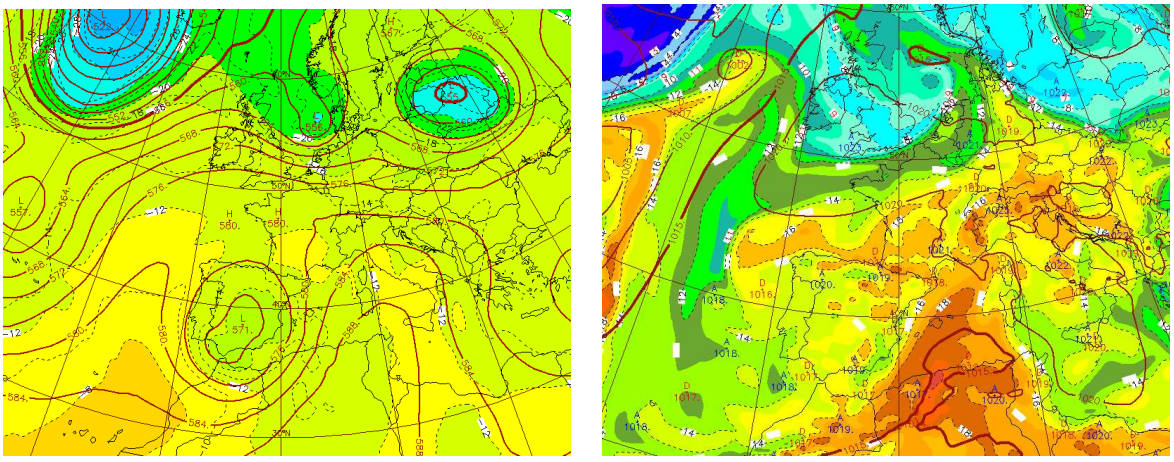

(a) (b)

Figure 1: Synoptic patterns: ARPEGE analysis at 12 UTC, (a) geopotential and temperature at 500 hPa, (b) mean sea level pressure and wet bulb potential temperature at 850 hPa.

In order to better identify mechanisms responsible for the initiation and evolution of this severe thunderstorm, three mesoscale numerical models have been used (Méso-NH, WRF and MM5) to perform an ensemble of 9 control simulations. In addition, these experiments have

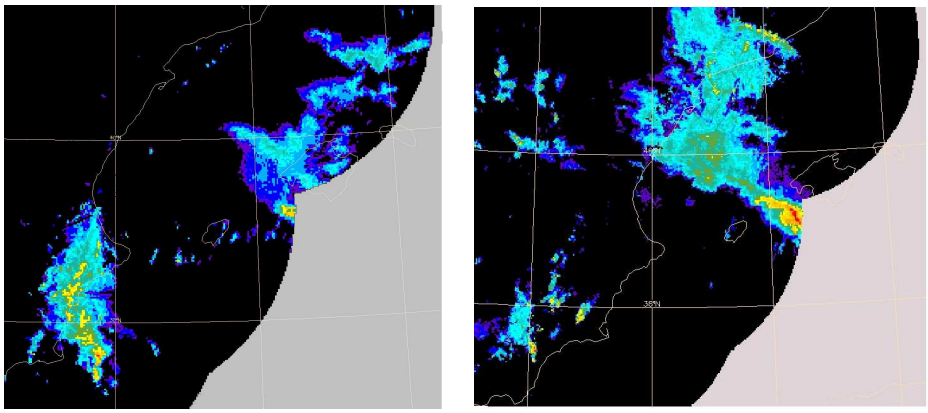

(a) 9h UTC (b) 15 UTC

Figure 2: Radar reflectivities at (a) 9 UTC and (b) 15 UTC.

been carried out for the purpose of investigating on the one hand, influences of models parameterizations, and on the other hand, the role of initial and boundary conditions. This latter factor was analysed comparing simulations with and without grid nesting. All the experiments were achieved with a fine resolution mesh (between 2 and 2.4 km) centered over Mallorca and therefore without deep convection parameterization. Analyses rather than forecasts were used to provide the most realistic initial and boundary conditions.

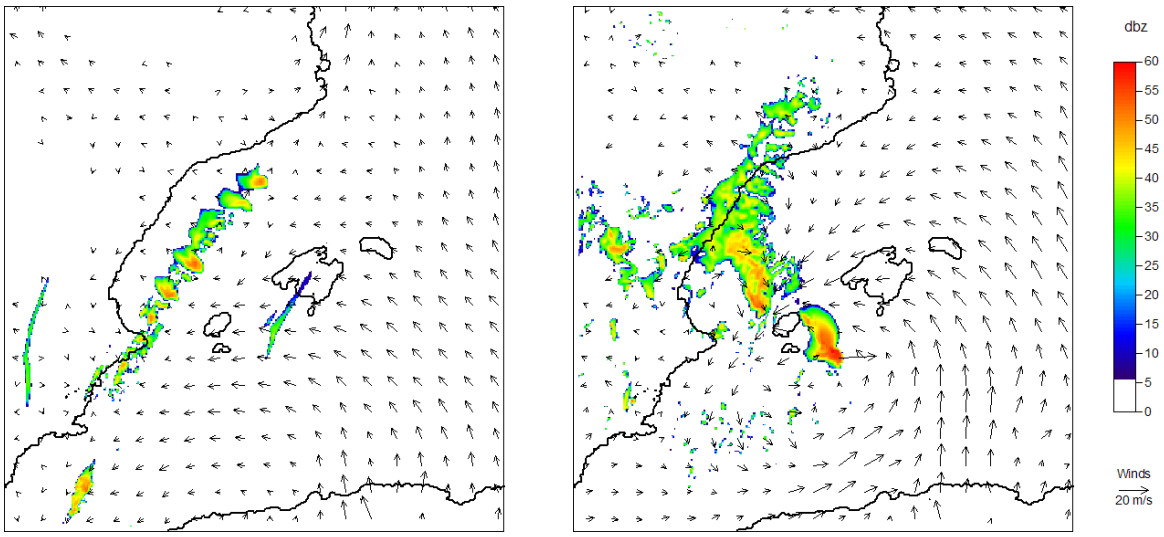

(a) 9 UTC (b) 15 UTC

Figure 3: Reflectivities at 800 hPa and winds at 925 hPa for WRF experiment forced by ECMWF analysis at (a) 9 UTC, (b) 15 UTC.

The analysis of the ensemble of experiments leads to the conclusion that the low-level convergence appears to be in this case the key element to explain the triggering of deep convection. The position of a low pressure area to the south of the Balearic archipelago in the lower troposphere is an important factor to enable a well located triggering of the storm. The experiment performed with WRF forced by ECMWF analysis succeeds in reproducing the squall line evolution with the best spatiotemporal representation. Reflectivities and low-level winds are displayed in figure 3 at 9 and 15 UTC. In the morning, this simulation triggers a convective cell to the south of Murcia, over an area with significant wind convergence. This thunderstorm later organizes in a linear structure and crosses the Mediterranean sea along the thermal boundary to reach

Mallorca around 16 UTC. The high sheared environment resulting from an easterly low-level flow overlied by strong southerly winds appears to be necessary to sustain the squall line.

Given the successful results of the Méso-NH experiment fed with ECMWF analysis -which simulates the squall line in remarkable agreement with remote sensing observations, despite a time lag-, further experiments have been carried out. An analysis of the internal structure and dynamics of convection confirms the squall line organization of the simulated convective system. In addition, a very high resolution simulation with a grid size of 600 meters, performed on a domain surrounding the squall line already formed, points out a bow-echo in reflectivities located in the southern sector of the squall line (figure 4-a). Near the bow apex and in other undulations of the squall line leading edge, where the rear inflow jet is severe, the highly detailed simulation allows to highlight vertical mesovortices enhanced by updrafts ahead of the gust front (figure 4-b). Even though the theory of such vortices genesis is extremely recent, they are known to be essential precursors of type II tornadoes, those associated with quasi-linear convective systems.

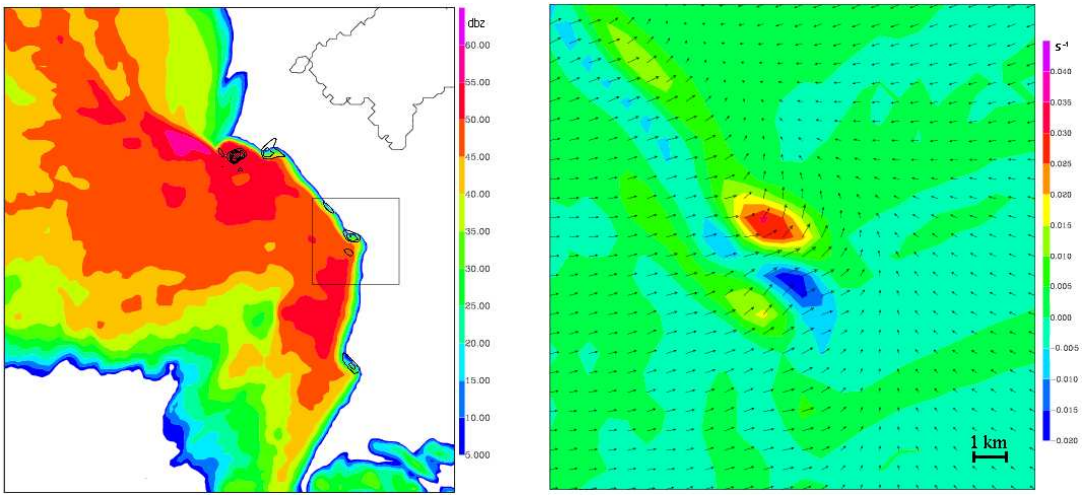

(a) (b)

Figure 4: Very high resolution simulation with Méso-NH and a 600 m grid size, at 12h30 UTC; (a) reflectivities with positive vertical vorticity at 200 m (contoured in black from 1.10^{-2} s^{-1} to 6.10^{-2} s^{-1} every 1.10^{-2} s^{-1}) and indication of (b) domain; (b) vertical vorticity and horizontal wind at 200 m.

Méso-NH simulations have been performed with several initial conditions from ECMWF, ARPEGE and ALADIN, and confirm the crucial effects of initial state on the numerical modeling. Failure of experiments initialized with ALADIN data is clearly due to a bad initial capture in analyses of the environment over the Mediterranean sea. Experiments fed with ECMWF and ARPEGE present closer low-level flows and achieve simulations with more realistic evolutions. However, differences in the low-level temperature fields lead to a best convective triggering with ARPEGE experiments, in which the front is associated with a stronger convergence of winds. In addition, the comparison of simulations performed with and without grid nesting indicates that on the whole, best results are obtained with a direct forcing by coarser analyses. Indeed, in experiments with grid nesting, stronger winds are simulated on the son domain as a consequence of a significant low-level pressure gradient imposed by boundary conditions. This observation proves the essential role exerted on this case by data assimilation to improve boundary conditions quality. Moreover, differences pointed out in experiments performed with Méso-NH, WRF and

MM5 with the same initial conditions indicate the benefits of a multi-model approach, since each one is characterized by its own physical and dynamical parameterizations.

Of particular importance is that the MM5 model is not able to trigger a convective cell offshore of Murcia, as opposed to the other models. In order to attempt to remedy this failure to correctly simulate the event, two different approaches have been considered. Since in the MM5 experiment, the lack of low-levels convergence seems to avoid an efficient convective triggering (figure 5-a), the first improvement was to assimilate pseudo-observations in order to synthetically generate a convergence line. Such observations are inspired from an experiment with Méso-NH forced by ARPEGE analyses in which initial stages of the convective cell are well captured. Only wind pseudo-observations are provided in the morning, at several levels in the planetary boundary layer, in order to initiate convection. Data assimilation of these pseudo-observations by the nudging method results in a well located convective triggering necessary to the further good evolution of the squall line (figure 5-b). Although the simulated squall line is slightly off to the west of Mallorca, it is very similar to observed radar reflectivities.

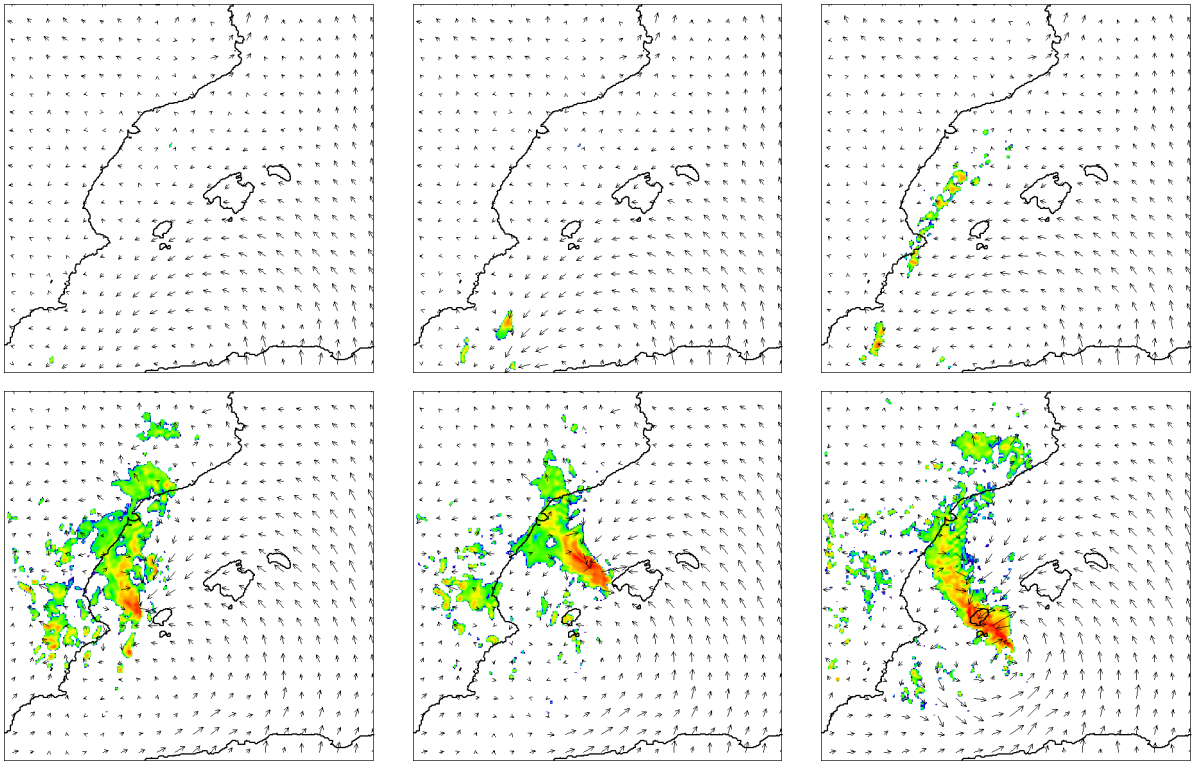

(a) (b) (c)

Figure 5: Reflectivities at 800 hPa and winds at 925 hPa (same scales as in figure 3) at 9 and 15 UTC for, (a) MM5 reference simulation, (b) simulation with data assimilation, (c) simulation with ETA planetary boundary layer scheme.

The second approach was to explore the sensitivity of the MM5 reference simulation to the planetary boundary layer scheme, since on the whole domain, the convection develops later than with other models. The substitution of MRF scheme daily used in UIB[1] "operational" forecast by ETA scheme leads to significant improvements in the simulation. With this later scheme,

[1] UIB: Universitat de les Illes Balears

using an 1.5 order of closure and a prognostic equation to compute TKE[2], convection is favoured and the triggering of the squall line takes place with rather accurate spatiotemporal features (figure 5-c). The lower diffusion of vertical velocity patterns and a better representation of the moisture vertical profile in the first levels are crucial factors to this success.

Even though the triggering and the evolution of the squall line occurred over the sea, a simulation in which the Atlas orography is removed allows an interpretation of the effects of the mountain range on the low-level flow. This time, the reference was the experiment performed with WRF using grid nesting, which includes all the Atlas and whose triggering is rather correct. Since differences are not large between the two experiments, the Atlas orography is not a decisive factor to explain the easterly flow necessary to the convective triggering, more ascribable to the dynamic low over North Africa. However, the low pressure area downstream of Atlas mountains intensifies the convergence offshore of Murcia and improves the location of the simulated thunderstorm.

To conclude, the success of a numerical simulation to capture a severe convective event with a maritime initiation closely depends on a conjunction of factors from distinct scales. On the 4^{th} October 2007 event, in a favourable synoptic environment which has been identified, a mesoscale circulation was necessary to lead to the squall line triggering. Finally, the ability of mesoscale numerical models to reproduce such maritime convective event is highly dependant on initial condition accuracy, an ever-present challenge over the data-void Mediterranean basin.

[2]TKE: Turbulent Kinetic Energy

Résumé long

Les pays méditerranéens sont régulièrement concernés par des épisodes dévastateurs de convection profonde, notamment en automne, période durant laquelle la température de la mer est élevée. La majorité de ces orages sont initiés par le relief présent autour du bassin méditerranéen. Cependant, dans certains cas comme celui de la ligne de grains du 4 octobre 2007 qui affecta l'île de Majorque, des systèmes convectifs de méso-échelle se développent et évoluent sur la mer. L'objectif de cette étude est de modéliser à fine résolution cet épisode convectif grâce à une combinaison de trois modèles numériques alimentés par différentes conditions initiales et aux limites, dans le but de comprendre l'environnement météorologique qui a permis de générer une telle ligne de grains.

Le 4 octobre 2007, les conditions météorologiques étaient favorables à la formation d'orages dans l'ouest du bassin méditerranéen. En altitude, une goutte froide située sur la péninsule Ibérique (figure 1-a) était associée à une profonde anomalie de tropopause bordée par une branche de jet divergente. En basses couches, une zone de forte baroclinie présentant une structure de catafront s'étendait le long de la côte est espagnole (figure 1-b) et délimitait une masse d'air chaude et humide située au-dessus de la mer. Dans cet environnement, un cellule convective s'est formée en début de matinée au large de Murcia, ville située au sud-est de l'Espagne (figure 2-a). Après une phase quasi-stationnaire durant laquelle l'orage présentait une structure en forme de V, ce dernier s'est progressivement organisé en ligne de grains en se déplaçant vers le nord-est (figure 2-b). En arrivant sur la ville de Palma, cette ligne de grains a engendré de puissantes rafales, des pluies torrentielles, et plusieurs tornades d'intensité F2-F3 sur l'échelle de Fujita, entraînant la mort d'une personne et d'importants dégâts dans la partie sud-ouest de l'île.

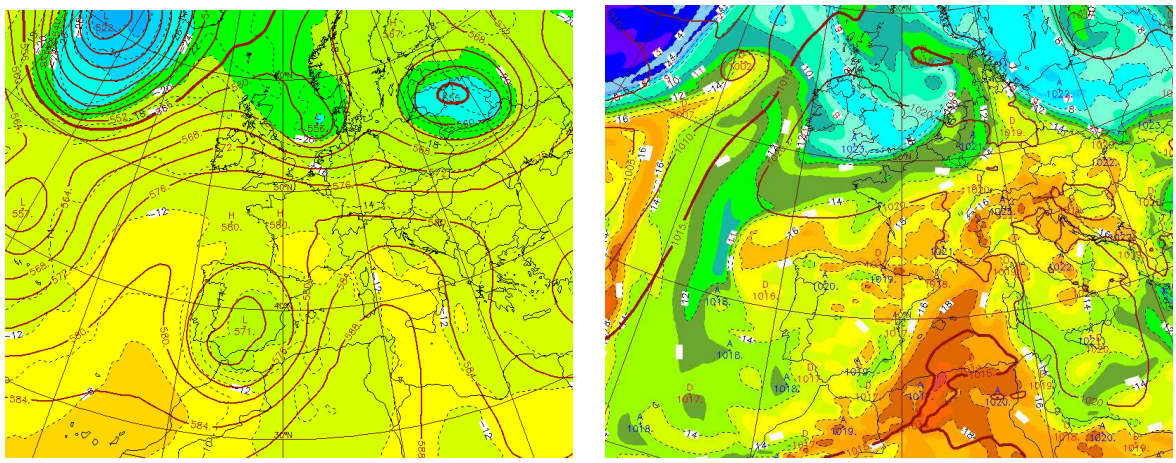

(a) (b)

Figure 1: Conditions synoptiques : analyse ARPEGE à 12 UTC (a) géopotentiel et température à 500 hPa, (b) Pmer et θ'w à 850 hPa.

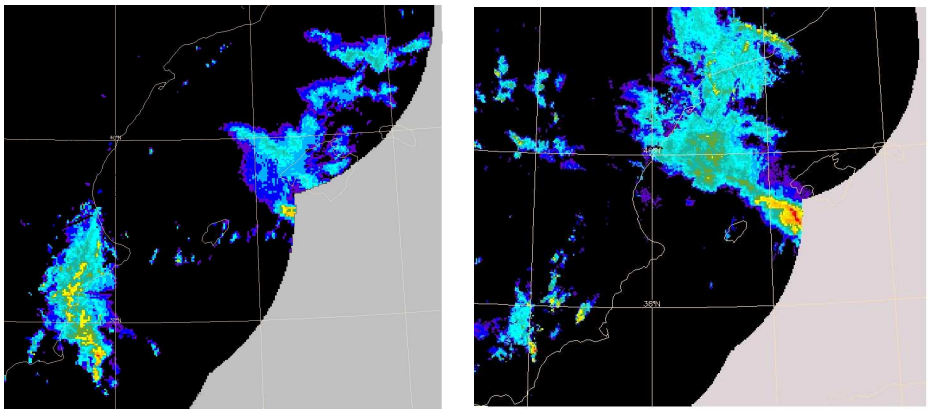

(a) 9h UTC (b) 15 UTC

Figure 2: Réfléctivités radar à (a) 9 UTC, (b) 15 UTC.

Afin de pouvoir identifier les mécanismes responsables de l'initiation et de l'évolution de cette ligne de grains, trois modèles numériques de méso-échelle ont été utililisés (Méso-NH, WRF et MM5) et ont permis de réaliser un ensemble de 9 simulations de contrôle. Ces expériences avaient pour objectifs de déterminer d'une part l'influence des paramétrisations de chaque modèle, et d'autre part l'importance des conditions initiales et aux limites. Ce dernier effet a été analysé via une comparaison de simulations avec et sans grid nesting. Toutes les expériences ont été réalisées sur un domaine centré sur Majorque, avec une maille de haute résolution comprise entre 2 et 2.4 km, donc suffisamment fine pour résoudre explicitement la convection profonde. Dans une configuration d'étude de cas, les analyses ont été utilisées pour fournir les conditions aux limites les plus réalistes possibles.

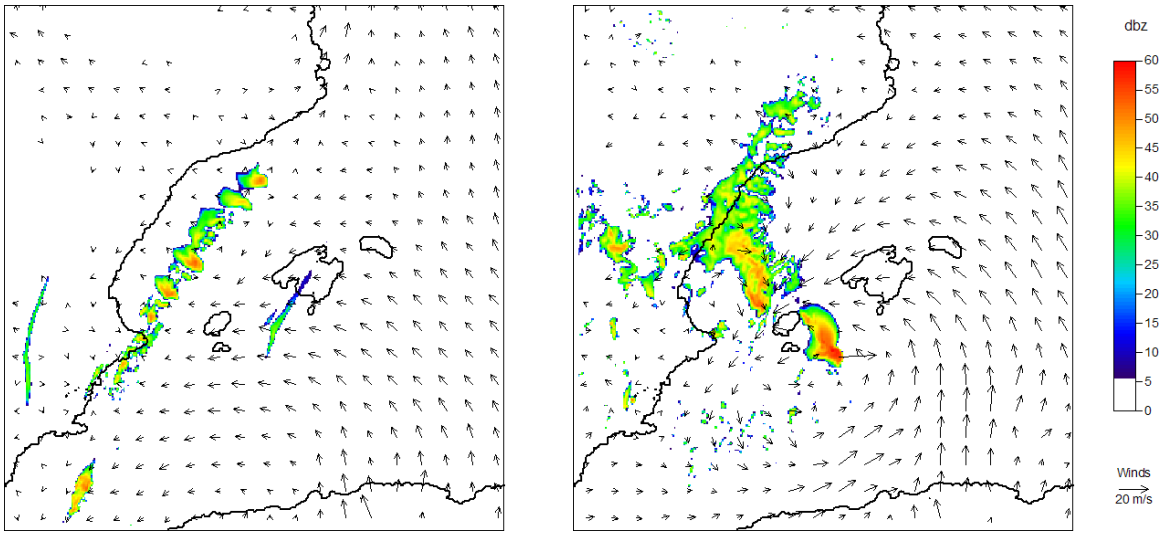

(a) 9 UTC (b) 15 UTC

Figure 3: Réfléctivités à 800 hPa et vents à 925 hPa pour l'expérience avec WRF forcé par les analyses ECMWF, (a) à 9 UTC, (b) à 15 UTC.

L'analyse de l'ensemble de simulations ainsi obtenu conduit à la conclusion que dans ce cas, la convergence de basses couches est un facteur déterminant pour expliquer le déclenchement de la convection profonde. La position d'une dépression relative en basses couches au sud des îles Baléares est un élément important pour permettre une bonne localisation de l'initiation convective. L'expérience réalisée avec le modèle WRF forcé par les analyses ECMWF parvient

à reproduire l'evolution de la ligne de grains dans les meilleures conditions spatio-temporelles. Les réfléctivités radar et les vents de basses couches sont présentés en figure 3, à 9 et 15 UTC. Cette simulation génère un orage en début de matinéee grâce à la convergence des vents au sud de Murcia. Par la suite, cet orage acquiert une structure linéaire qui se déplace au dessus de la Méditerranée le long de la frontière thermique, pour atteindre Majorque à 16 UTC. Le fort cisaillement dans les premiers kilomètres de la troposphère entre le flux d'est de basses couches et les forts vents de dominante sud en altitude, apparait être nécessaire pour maintenir la ligne de grains.

Grâce à la simulation combinant Méso-NH avec les analyses ECMWF, qui parvient à créer un structure convective très proche des observations radars et satellites malgré un décalage temporel, de investigations plus précises ont été menées. L'analyse des dynamiques internes du système convectif démontre l'organisation en ligne de grains de la convection modélisée. De plus, une simulation réalisée à une résolution de 600 mètres sur un domaine entourant la ligne de grains déjà formée, met en évidence une structure de bow echo dans la partie sud du système convectif (figure 4-a). Proche de la pointe du bow echo, comme dans d'autres ondulations du bord d'attaque de la ligne de grains où les mouvements descendants sont puissants, le haut degré de détails de la simulation permet de détecter des mesovortex verticaux engendrés par des ascendances à l'avant du front de rafales (figure 4-b). Même si la théorie expliquant la naissance de tels vortex est très récente, ils sont connus pour être des précurseurs essentiels de la naissance de tornades de type II, celles associées aux systèmes convectifs quasi-linéaires.

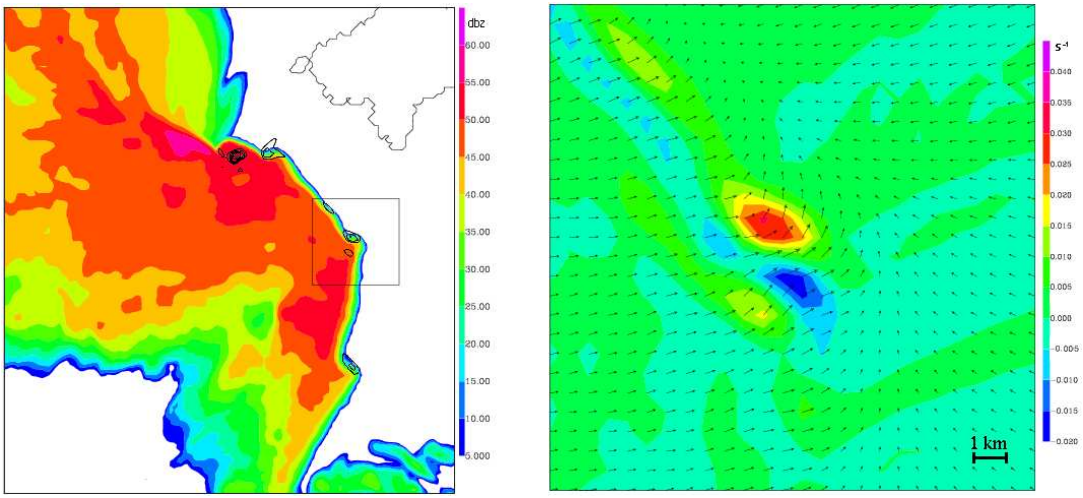

(a) (b)

Figure 4: Simulation à très haute résolution avec Méso-NH et une grille de 600 m de côté à 12h30 UTC; (a) réfléctivités et vorticité verticale positive à 200 m (contours en noir de 1.10^{-2} s^{-1} à 6.10^{-2} s^{-1} chaque 1.10^{-2} s^{-1}) et indication du domaine (b); (b) vorticité verticale et vent horizontaux à 200 m.

Les simluations avec Méso-NH ont été effectuées avec plusieurs conditions initiales, provenant des modèles ECMWF, ARPEGE et ALADIN, et démontrent l'importance de l'état initial sur la modélisation numérique. L'echec des simulations alimentées par les données ALADIN est clairement dû à une mauvaise représentation de l'environnement initial sur la mer Méditerranée dans les analyses. Les expériences menéees avec ECMWF et ARPEGE présentent un flux de basses couches assez concordant et aboutissent à des représentations plus fidèles de la situation. Cependant, des différences dans les champs de températures potentielles conduisent à une meilleure initiation dans les expériences alimentées avec ARPEGE, dans lesquelles le front est

associé à une convergence des vents plus marquée. Par ailleurs, la comparaison des simulations avec et sans grid nesting indique que dans l'ensemble, les meilleurs résultats sont obtenus quand le domaine de haute résolution est directement forcé par les analyses. En effet, dans les expériences avec un domaine intermédiaire, l'intensité des vents est excessive dans le domaine fils, en conséquence d'un trop fort gradient de pression imposé par les conditions aux limites en basses couches. Cette remarque prouve le rôle essentiel joué par l'assimilation de données dans ce cas pour améliorer la qualité des conditions aux limites. De plus, les différences mises en évidence dans les modélisations réalisées par Méso-NH, WRF et MM5 avec les mêmes conditions initiales démontrent les avantages d'une approche multi-modèles, puisque chacun est caractérisé par ses propres paramétrisations physiques et dynamiques.

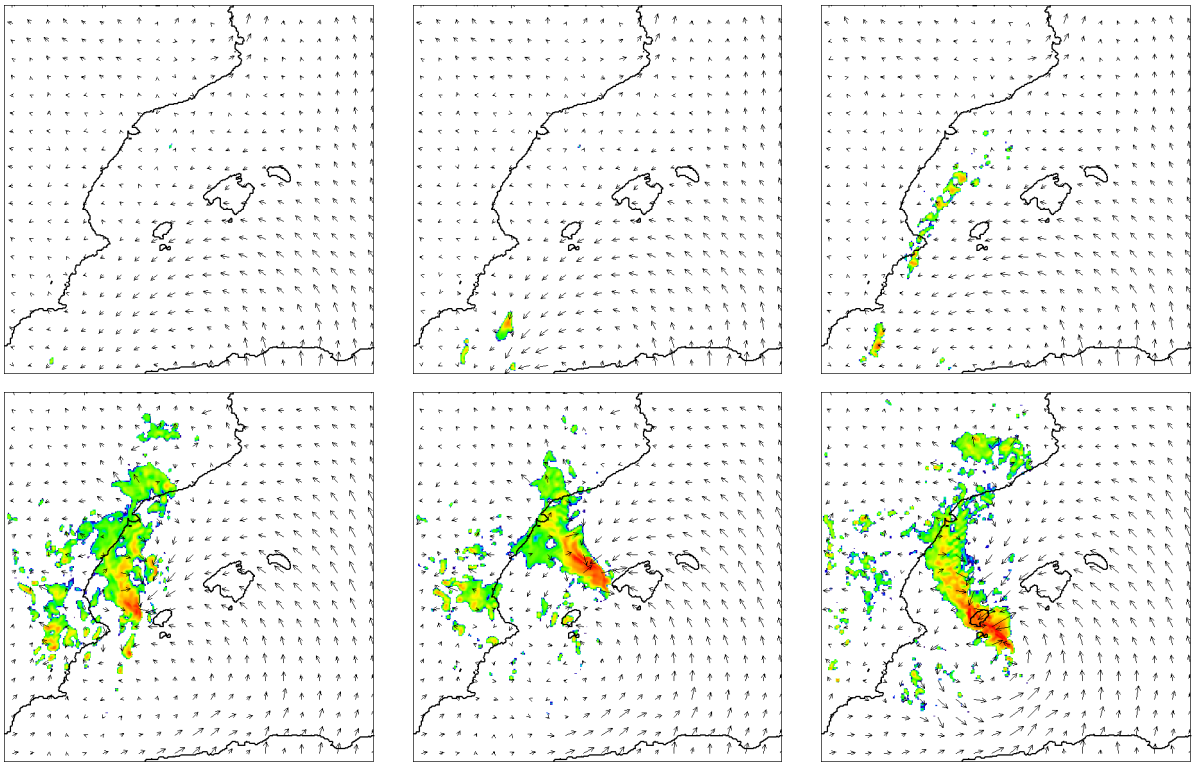

(a) (b) (c)

Figure 5: Réfléctivités à 800 hPa et vents à 925 hPa (même échelle qu'en figure 3) à 9 et 15 UTC pour (a) la simulation MM5 de référence , (b) la simulation avec assimilation de données, (c) la simulation avec le schéma de couche limite ETA.

Un fait particulièrement remarquable est que MM5 ne parvient pas initier une cellule convective au large de Murcia, comme le font les deux autres modèles. Dans le but de remédier à ce défaut, deux différentes approches ont été envisagées. Comme le manque de convergence de basses couches semblait empêcher la naissance de l'orage dans la matinée (figure 5-a), la première piste d'amélioration a été d'assimiler des pseudo-observations dans le but de générer une ligne de convergence. Ces observations sont inspirées de la simulation de Méso-NH forcé par les analyses ARPEGE, dans laquelle la première phase de la naissance de la ligne de grains est bien représentée. Seulement des pseudo-observations de vents sont fournies le matin à plusieurs niveaux dans la couche limite. L'assimilation de ces pseudo-observations par une méthode de nudging aboutit à un résultat très satisfaisant caractérisé par la présence de la cellule convetive initiale au bon emplacement (figure 5-b). Par la suite, bien que la ligne de grains simulée soit légèrement trop à l'ouest de Majorque, elle présente une structure vraiment similaire aux réflectivités radar observées.

La seconde approche a été de déterminer la sensibilité de la simulation MM5 de référence au schéma de couche limite, puisque dans l'ensemble du domaine, la convection se développe plus tard qu'avec les autres modèles. La substitution du schéma MRF utilisé quotidiennement dans la prévision "opérationnelle" de l'UIB[3] par le schéma ETA conduit à une amélioration significative de la simulation. Avec ce dernier schéma, utilisant une fermeture à l'ordre 1.5 et une équation pronostique pour calculer la TKE[4], la convection est favorisée et le déclenchement de la ligne de grains apparaît dans des conditions spatio-temporelles plutôt correctes, bien qu'il ait lieu légèrement trop au sud (figure 5-c). La plus faible diffusion de l'énergie de méso-échelle vers les processus turbulents et une meilleure représentation du profile vertical d'humidité en basses couches sont les clés de cette amélioration.

Même si l'initiation de la convection se passe dans une zone maritime, une expérience de sensibilité dans laquelle l'orographie de l'Atlas est supprimée a permis d'interpréter l'influence de cette chaîne de montagnes sur le flux de basses couches. Dans ce cas, l'expérience de référence est la simulation réalisée en grid nesting avec WRF, dont le domaine père inclut entièrement l'Atlas, et dont la représentation de l'initiation convective est plutôt satisfaisante. Finalement, les différences sont relativement minimes une fois le relief africain supprimé, ce qui prouve que le flux d'est nécessaire au déclenchement de la convection est majoritairement attribuable à une dépression dynamique centrée sur l'Afrique du nord. Cependant, la zone de basses pressions en aval des montagnes de l'Atlas intensifie la convergence au large de Murcia et détermine plus précisément la localisation de l'orage.

En conclusion, le succès de la modélisation numérique d'un épisode fortement convectif ayant une initiation maritime est étroitement lié à une intéraction de facteurs de différentes échelles. Le 4 octobre 2007, sous une situation synopique favorable bien identifiée, une circulation de méso-échelle était nécessaire pour parvenir à initier la ligne de grains. Finalement, la capacité des modèles numériques à reproduire de tels épisodes convectifs est fortement dépendante de la précision des conditions intitiales, toujours difficile à évaluer au-dessus du bassin Méditerranéen.

[3]UIB: Universitat de les Illes Balears
[4]TKE: Turbulent Kinetic Energy

Contents

Introduction

The Mediterranean basin is regularly affected by severe weather associated with deep convection. All western surrounding countries have known catastrophic flash-flood events often characterized by quasi stationary systems. The role played by the orography is usually fundamental to explain the triggering and the sustainment of such thunderstorms. However, some Mediterranean severe thunderstorms develop and mature over the sea, without direct orographic forcing. On their path, these mesoscale convective systems can also affect populated areas. A good and recent example of this kind of convection is the severe thunderstorm that crossed the island of Mallorca on the afternoon of 4^{th} October 2007. Generated early in the morning offshore of Murcia, this storm organized progressively into a squall line structure as it moved northeastwards. Arriving in Palma city, the squall line was accompanied by severe gusts, heavy rain and several tornadoes, leading to significant damages in the southwestern part of the island, and eventually to one fatality.

The initiation, mode and evolution of convection in these maritime events depend on both synoptic and mesoscale features, some of them convectively generated. Representing such interaction is a real challenge for numerical models used in weather forcasting. Mesoscale numerical models have already shown their ability to locate heavy precipitating events, especially in areas where orographic forcing is important (Romero et al. 2001; Ducrocq et al. 2002; Nuissier et al. 2008). Much less studies have been focused on the intricate issue of convective initiation over the Mediterranean sea, where only few observed data are available, resulting in large uncertainties in models analyses.

The aims of this research project is to simulate the case of 4^{th} October 2007 with a combination of three numerical models using several initial and boundary conditions. This set of simulations will help identifying which mechanisms are most relevant to obtain a good numerical spatiotemporal representation of the squall line. The best simulations are expected to provide interesting comprehensive elements of squall lines dynamics and structure. This study also allows to assess initial and boundary conditions influences as well as model parameterization impacts on the modeling framework. Another objective is to test simulation improvements by assimilating synthetically generated observations corresponding to mesoscale features, in order to remedy the lack of data over the sea. The idea is to assimilate pseudo-observations of plausible structures that are believed to be necessary to the convective initiation.

This paper is organized as follows. In the first chapter, some elements of deep convection are reviewed with particular attention paid to squall lines physics and dynamics. The second chapter illustrates the case of 4^{th} October 2007 with a study of observed data. Then, a chapter is devoted to explain methods used and parameterizations chosen in each experiment with three mesoscale numerical models: Méso-NH, WRF and MM5. The fourth chapter details results of simulations carried out with the three models. Numerical possibilities of each one will be exploited to complete this comparative study. Méso-NH, which can be run with several initial and boundary conditions available, will guide the analysis of the coupling impact in the simulation of this particular event. MM5, which has its own data assimilation scheme will be used to improve

simulations by means of additional pseudo-observations. Finally, some sensitivity experiments will be performed with MM5 and WRF, with the aim of completing the event understanding. On the one hand, the impact of the planetary boundary layer scheme on convection triggering will be analysed, and on the other hand, the Atlas orography influence on the flow circulation will be determined.

Chapter 1

Mesoscale convective systems and squall lines

1.1 Mediterranean mesoscale convective systems

Depending on synoptic and mesoscale features, different convective modes can develop in the atmosphere. When the instability is prounounced, specific patterns can lead to several thunderstorms organised in MCS[1]. Their structures vary depending on the combination of many atmospheric and surface features, which must be taken into account to explain these phenomena. MCS dynamics are more complex than those of individual thunderstorms, especially due to the fact that these systems often contain a large region of stratiform precipitation. Houze (1993) defines a MCS as a cloud system that occurs in connection with an ensemble of thunderstorms and produces a contiguous precipitation area of 100 km or more in horizontal scale in at least one direction. However, their size can reach more than 1000 km in tropical latitudes. The most famous kind of MCS, which presents a well organized structure is the squall line. A particular description of favourable meteorological conditions for squall lines development is discussed in section 1.3, as well as a description of their stucture and dynamics. Other MCS types are also well documented, as a V-shaped multicellular thunderstorm, easily identifiable with satellite imagery. Most devastating flash-flood events can be attributed to quasi-stationary MCS. All coastal areas of the western Mediterranean basin can be affected by extreme events like those of Vaison-la-Romaine in southern France on 22 September 1992, Gandia in Central Valencia on 3 November 1987 where more than 800 mm were recorded in 24 hours, or like the catastrophic floods of the Piedmont region in northwestern Italy on 5 November 1994.

Western coastal Mediterranean regions are known to be particularly favourable to MCS development often tied to heavy rainfall events especially under a specific type of weather regimes. Necessary conditions leading to these phenomena are on the one hand an important low-level flow of moisture coming from the sea, and on the other hand a large scale trough over France and Spain associated with a divergent jet streak aloft. It is frequent that small MCS develop over the Alboran Sea during the fall, as the sea is quite warm after the high insolation throughout the summer. Then they move towards the Spanish Mediterranean littoral staying for a long time close to the coast line. To become stationary, MCS require a mesoscale mechanism which releases the instability at the same location during several hours. Mesoscale ingredients necessary to trigger and sustain Mediterranean convection have been extensively analysed by means of numerical models. Particularly, the orography plays a crucial role when a moist and conditionally unstable low-level jet impinges against coastal mountains (Ducrocq et al. 2008). Moreover, Romero et al. (2001) demonstrate the prevailing role of convectively induced cold pools and outflows to explain the propagation of convective systems.

[1] MCS: Mesoscale Convective System

1.2 Essential elements in deep convection

1.2.1 Convective instability

In order to forecast thunderstorms, it is fundamental to assess the atmospheric instability. Two thermodynamical parameters are commonly used, the CAPE[2] and the CIN[3]. The CAPE describes the potential buoyancy available for an idealised rising of low-level air parcels and thus denotes the instability of the troposphere. This parameter is calculated by the following means:

$$CAPE = \int_{LFC}^{LNB} \beta dz \quad \text{with} \quad \beta = -g\frac{\rho_p - \rho_{env}}{\rho_{env}} \tag{1.1}$$

where LFC is the level of free convection, LNB the level of neutral bouyancy, and β the parcel bouyancy depending on the difference between the parcel and the environment density (respectively ρ_p and ρ_{env}). Even if it often exceeds 1000 $J.kg^{-1}$ in thunderstorm environments, in Mediterranean regions a CAPE of only few hundreds $J.kg^{-1}$ may be enough to support severe convection.

Before using the energy available in the troposphere, the parcel has to reach its level of free convection. The CIN parameter describes the amount of energy necessary for a rising parcel to overcome a stable surface layer. It is defined by the following formula:

$$CIN = -\int_{0}^{LFC} \beta dz \tag{1.2}$$

An environment with a strong CIN inhibits convective developments. However, if a synoptic feature or a mesoscale element succeeds in breaking the low-level stable layer, it acts as a convection triggering, releasing the accumulated CAPE. This kind of scenario is known to lead to severe convective cells formation.

1.2.2 Vertical wind shear

Vertical wind shear refers to the variation of horizontal wind over vertical distances, calculated as a gradient. It can be seen as horizontal vorticity. It significantly influences what convective mode is likely to develop. In deep convection, a sheared environment is prone to maintain the system as updrafts and downdrafts can be separated. On the contrary, in unsheared environment, rainfall reduces steadily convective motions.

If we consider a bidimensional flow (x-z), the Bousinesq inviscid equation governig the vorticity becomes:

$$\frac{d\eta}{dt} = -\frac{\delta\beta}{\delta x} \quad \text{with} \quad \eta = \frac{\delta u}{\delta z} - \frac{\delta w}{\delta x} \tag{1.3}$$

This equation indicates that the horizontal vorticity η depends on the horizontal gradient of buoyancy β. If there is an updraft in a flow with no shear, as represented in figure 1.1-a, the buoyancy distribution creates a positive vorticity on the right side and a negative on the left side of the updraft, in equal amouts. Thus the axis of the updraft is vertical. If we add to this scenario a shear environment as in figure 1.1-c, it will lean the updraft downshear as the positive vorticity on the right side become stronger. This tilt is modulated by the possible presence of a cold pool generating negative vorticity at its nose due to the buoyancy gradient (Eq. 1.3). Air rising is under the influence of this negative vortex, which without shear causes updraft to lean over the cold pool (figure 1.1-b). The scenario known as the optimal case is obtained when the

[2]CAPE: Convective Available Potential Energy
[3]CIN: Convective Inhibition

positive vorticity associated with the low-level shear just balances the generation of negative vorticity by the cold pool as shown in figure 1.1-d.

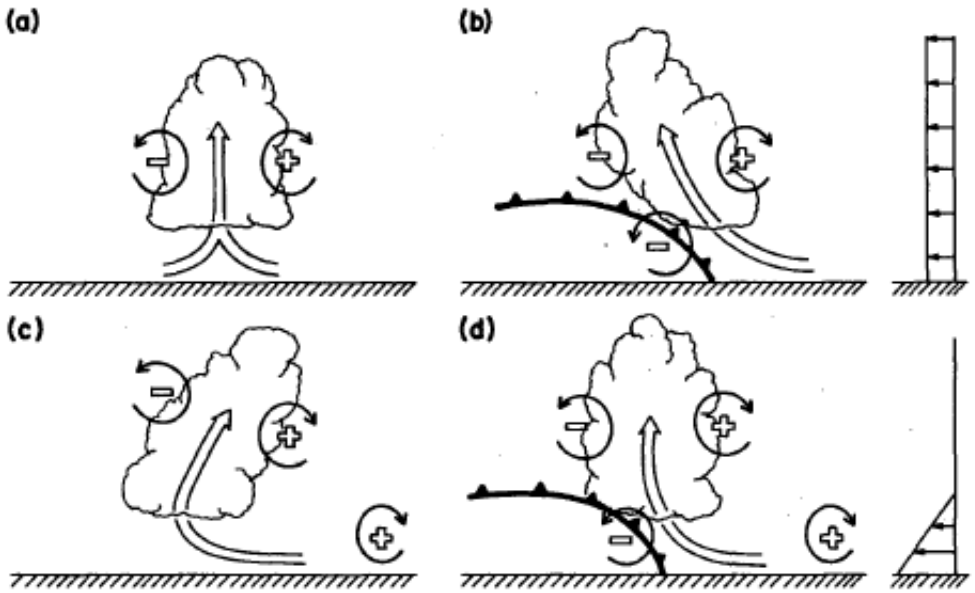

Figure 1.1: Influence of wind shear and cold pools on buoyant updraft, from Rotunno et al. (1988).

The shear orientation is also relevant for cell organization in deep convection. Indeed, a unidirectional shear is favourable to multicellular thunderstorms as for example V-shaped structures. A veering shear is known to increase the likelihood of supercells, the most dangerous kind of thunderstorm often able to generate tornadoes.

1.3 Squall lines description

1.3.1 Definition

Probably the most commonly observed and studied form of mesoscale convective system is the squall line. According to the simplest definition, a squall line corresponds to any line of convective cells. Its length can vary from few tens of kilometers to 1000 km, so there is not a precise size definition. Squall lines are usually composed of a series of ordinary cells spread along and behind the leading edge of the system. However, a squall line may also be composed of several supercells and there may be bow-shaped segments of convective cells embedded in the line. Supercells and bow echoes are the most important cause of severe weather within squall lines, often accompanied by hail and tornadoes.

Squall lines can form by several means. They often originate as a scattered line of convective cells merging during their evolution, but they also may be triggered directly as a line. This latter scenario is especially likely when there is a strong large-scale or mesoscale forcing, for example with a cold front or a convergence line. The following descriptions of squall lines physics and dynamics are mainly based on Hane (1986) and Houze (1993) studies, and include elements exposed in the COMET[4] program.

[4]COMET: Cooperative Program for Operational Meteorology, Education and Training

1.3.2 Synoptic settings and mesoscale ingredients

1.3.2.1 Favourable environments

Synoptic conditions necessary for the formation of squall lines include those favorable to the formation of strong thunderstorms. However, there are specific features which influence the linear organization of convection. The ideal vertical profile is well identified, with a warm and moist air mass at low-levels, overlied by cold air aloft, that creates convective instability. Moreover, a dry layer just above the low-level moist area favours the line development if this dry air overtakes as surface front. The evaporation rate of rainfall raises into this dry air, leading to cooling and consequently to stronger downdrafts. If the vertical profile presents a low-level inversion, it increases the CIN and inhibits the formation of deep convection early in the morning, but when the convection begins, it provides an important amout of kinetic energy to the squall line.

1.3.2.2 Squall lines triggering

The kind of profile previously described is however not sufficient to explain squall lines formation, since a way to release the instability must be present. Several mechanisms able to trigger convection can be underlined. A common initiating mechanism is the convergence along a front, especially along a cold front often associated with synoptic scale systems. As shown by Browning (1986), convective organization is favoured if the cold front is a katafront since the descending motion ahead of the front can produce a dry layer that enhances deep convection. He also constated that almost all squall lines occur in the warm sector, ahead of a cold front. Another mechanism able to release instability is the generation of vertical motion as a consequence of upper-level disturbances corresponding to PV[5] anomalies. Besides, we can point out the important role played by earlier convection, leaving perturbed areas of pressure and cold pools near the ground. We can add to this list the orography, which also have a relevant influence on the trigerring of deep convection in mountainous regions, as it transforms horizontal wind into updraft. In its mature stage, the squall line creates its own mechanism to lift the warm and moist air, with the convergence area along the gust front.

1.3.2.3 Squall lines longevity

Squall lines display a characteristic lifecycle, starting as a narrow band of intense convective cells and evolving steadily to a broader and weaker system. Squall lines do not need vertical wind shear to be formed, but a sheared environment helps to sustain the line organization and consequently to increase the system longevity. The most useful parameter to estimate the shear environment controlling squall line structure and evolution is the component of low-level shear perpendicular to the line orientation.

The magnitude of the low-levels vertical shear of horizontal wind plays a relevant role in the squall line longevity. For mid latitudes environments, the line-normal shear magnitude between the ground and 3 km can be classified in weak (less than 10 $m.s^{-1}$), moderate (from 10 to 18 $m.s^{-1}$) and strong shear (greater than 18 $m.s^{-1}$). Weak shear environments produce squall lines that spread quickly and weaken after few hours, whereas stronger shear environments, able to balance the horizontal vorticity generated by the cold pool, are favourable to more long-lived lines composed of stronger cells and sometimes bow echoes. The wind shear above 3 km have also an influence on the squall line organization but weaker than at low-levels. Depending on its particular orientation, the impact of low-level shear may strengthen or decrease.

[5]PV: Potential Vorticity

1.3.3 Internal structure and dynamics

A conceptual model based on many observational studies of squall lines has been established and is displayed in figure 1.2, which presents a cross section perpendicular to the axis of the line. This scheme corresponds to the mature stage of a squall line. Two parts are clearly identifiable, the convective and the stratiform regions. This latter stretches over a large area at the rear of the system whose size often reaches few hundreds kilometers.

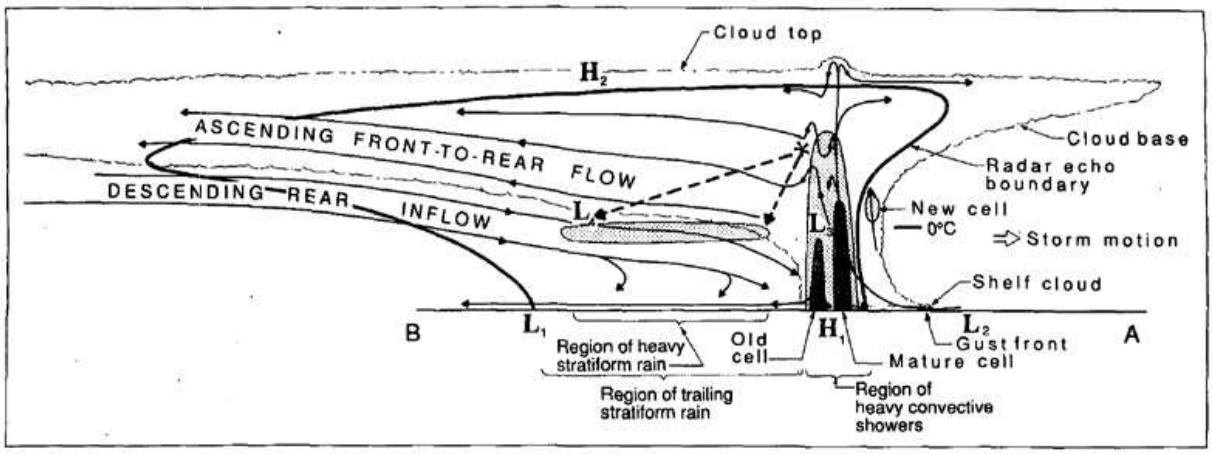

Figure 1.2: Conceptual model of a squall line, from Houze (1993).

The convective part is characterized by powerful updrafts, leading to heavy rain showers. The arrangement of cells in a perpendicular section is similar to the one present in multicellular thunderstorm, with a constant formation of new convective cells on the edge of the intense rainfall area, corresponding to the mature cell. In this cell, vertical updrafts are intense and can penetrate in the stratosphere where overshoots are commonly observed. Downdrafts associated with rainfall favour new cells development above the gustfront. Following the mature cell, old cells are steadily incorporated into the stratiform part.

At the beginning of the squall line life cycle, the stratiform part does not exist but progressively forms as the old cells get advected rearwards. However, its presence is fundamental for the squall line development and maintaining, allowing to link line cells. Indeed, the gust front necessary to new cells formation is enhanced by a mesoscale circulation guided by the stratiform part, called Rear Inflow Jet (RIJ). This organized dry air flow between stratiform and convective parts is absent in an isolated multicellular thunderstorm. The mechanism leading to precipitation in the stratiform region can be better explained with the figure 1.3. Ice particles produced by the convective part are spread across the stratiform area. The fall of these particles is slowed down by weak updrafts, that allows their growth by Bergeron effect. Once melted, ice particles fall to the ground as rain, partly evaporated in the dry air coming under the stratiform part. In a transition area just at the rear of the convective region, strong downdrafts avoid the particles growth, therefore rainfall is weaker in this area.

The pressure field observed in squall lines is characterized by several lows and highs noted as L and H in figure 1.2. Below the convective part, a surface high (H_1) is a consequence of cooling due to rainfall evaporation. A wake low (L_1) is always observed on the trailing edge

of the stratiform region and has also an hydrostatic nature. There is a consensus that this surface warmth results from subsidence, but there are different ideas regarding the cause of the subsidence. According to Haertel and Johnson (2000), the conceptual model of the squall line mesohigh–wake low couplet is as a quasi linear response to low-level cooling associated with stratiform precipitation. Besides, a pre-squall mesolow (L_2) is often noted as a response to a downwards flow at mid and upper-levels ahead. Two other mesolows in mid tropospheric levels are the consequence of the positive buoyancy in the convective part (L_3) like in the stratiform region (L_4). Obviously, they interact with the RIJ location. At least, a high (H_2) due to the ascending flow is present at the top of the system.

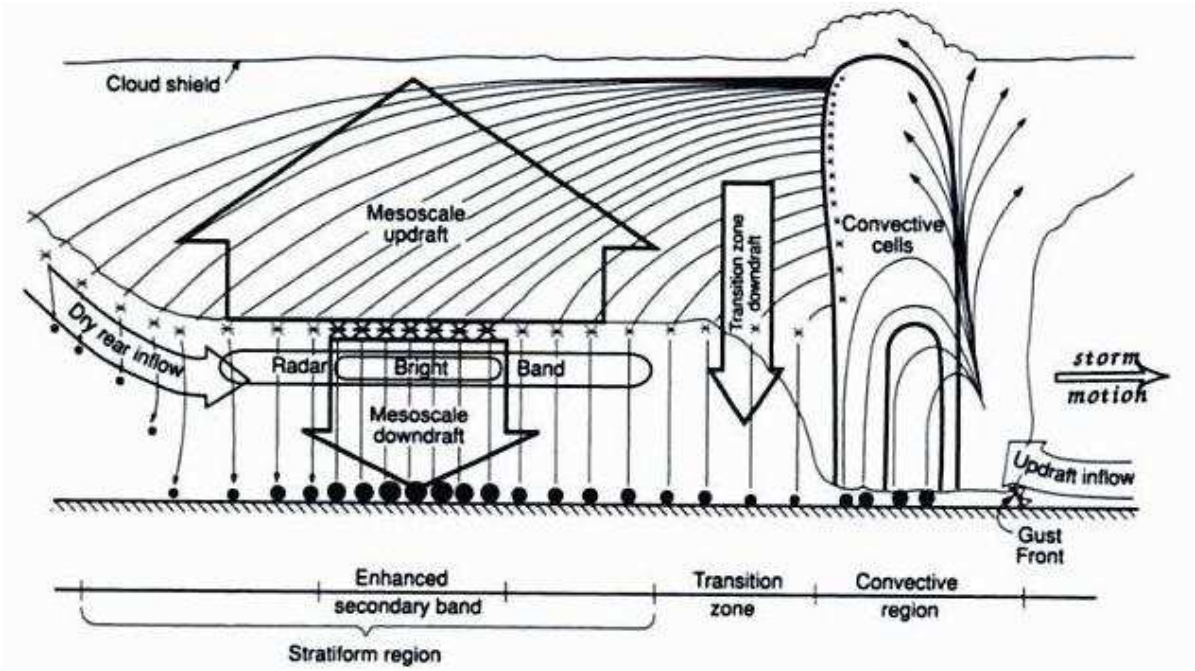

Figure 1.3: Dynamics of the stratiform region of a squall line, from Houze (1993).

1.3.4 Life cycle of a squall line

The life cycle of a squall line has a variable length ranging from few hours to two days in tropical latitudes. The schematic evolution of a typical mid-latitude squall line is shown in figure 1.4, in which radar reflectivities and low-level flows are displayed. In this figure the squall line is moving eastwards. During the early stages of the squall line evolution, several cells already exist but have mostly independent behaviours. Steadily, with the merge of cold pools, a linear structure appears at the leading edge. At low-levels, the flow is divergent below the cells since downdrafts spread at ground contact. With an easterly low-level flow, this mesoscale circulation creates a convergence area ahead of the line of cells, which strengthens upward motions in the convective part.

When the squall line becomes mature (t=2-6h), it sets up a mesoscale organization allowing its long life. The stronger cold pool enhances ascents in cells now able to create heavy rains. But the mature stage is also characterized by a stretched stratiform region at the rear of the convective region, responsible for weaker precipitation. A narrow region of very light precipitation, corresponding to the transition area, is usually observed between convective and stratiform

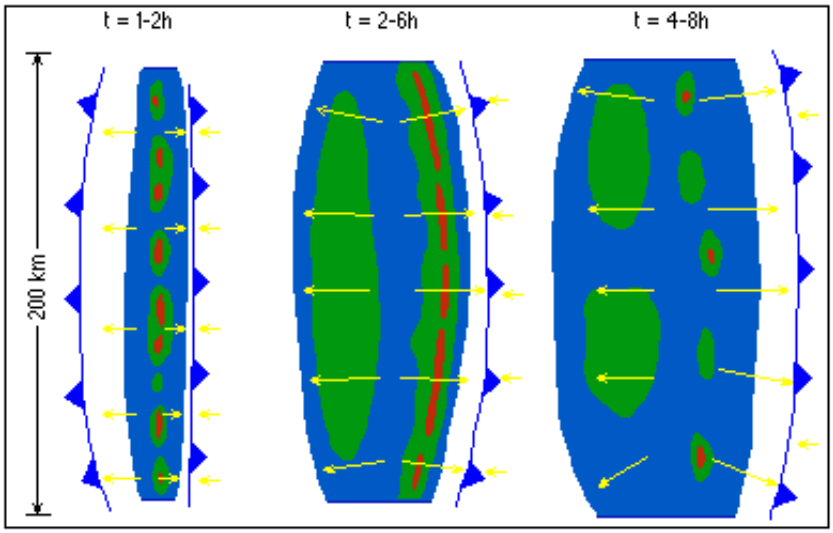

Figure 1.4: Life cycle of a squall line in a weak to moderate shear environment, from the COMET program.

parts. At this stage of their evolution, relatively short squall lines (less than 200 km) often develop regions of rotation at each end. Next, the cyclonic vortex will be favoured compared with the anticyclonic leading to an asymmetrical system.

The end of this life cycle (t=4-8h) is provoked when the cold pool, becoming too widespread, surges well ahead of the convective line avoiding efficient vertical motions. Although convective cells have weakened, the stratiform precipitation region may last for several hours.

1.3.5 Tornadoes within squall lines

Mechanisms for tornadogenesis are clasified in two categories. The genesis of type I tornadoes is tied to supercells dynamics and can lead to very powerful tornadoes. Although this kind of formation prevails, tornadoes are also observed in quasi-linear convective systems (QLCS) such as bow-shaped radar echoes. These tornadoes (type II) tend to be weaker and shorter-lived on average than those associated with supercell thunderstorms. However, this second type of genesis do not have to be neglected. An observational study led by Tessendorf and Trapp (2000) shows that it represents 20% of tornadic events in United States. Squall line tornadoes occur in lines devoid of supercells as well as in supercells embedded in a line. In United States where this topic is an important issue, the non supercells variety is known to be the most frequent form in conjunction with bow echoes.

Bow echo structure

A bow echo is a cluster of convective cells which progressively evolves in an arched line of thunderstorms, under the influence of a low-level cold pool. Bow echoes tend to develop when a moderate to strong wind shear affects the lower 2 to 3 km of the atmosphere. In mature stage, a bow echo contains a RIJ and associated downbursts account for a majority of damages resulting from convective non-tornadic winds. Light weak echo regions may be present on the leading edge of the bow reflectivity gradient marking the location of significant storm-relative inflow. As indicated in figure 1.5, tornadoes may occur on the cyclonic side of the jet of strong outflow winds.

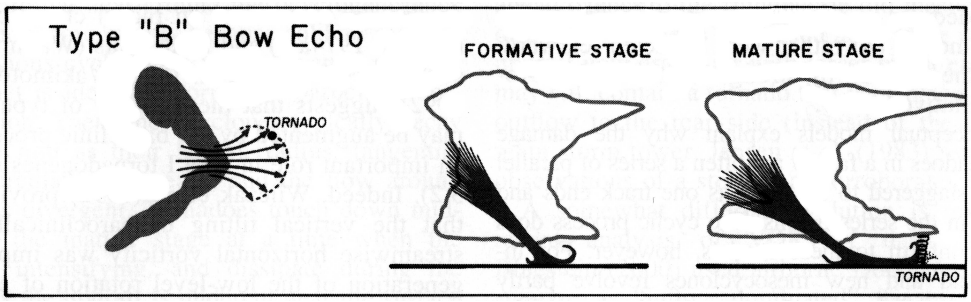

Figure 1.5: Tornado formation within a bow echo, from Fujita, 1985.

Mesovortices genesis

Numerical studies (Weisman and Trapp, 2003; Trapp and Weisman, 2003) demonstrate that the genesis of type II tornadoes are tied to an intensification of low-level mesovortices as in supercells tornadoes. Mosovortex genesis is initiated at low-levels by the titling of baroclinically generated horizontal vorticity. In mature QLCS, such horizontal vorticity located just rearward of the gust front is the consequence of the strong thermal gradient separating the cold pool from surrounding environment. As demontrated in a recent study (Atkins and St. Laurent, 2009-a), the strongest and therefore potentially most damaging mesovortices are those that develops where the gust front is locally enhanced by a descending RIJ. Mesovortices that forme prior to the RIJ produce weaker ground relative winds.

Vertical mesovortices have typical diameters of few kilometers, and later their intensity magnifies by means of a streching effect. Mesovortex strength depends upon the environmental shear, Coriolis forcing, and cold pool magnitude. According to Weisman and Trapp (2003), the Coriolis force has a direct impact on the enhancement of low-level cyclonic mesovortices and also in the anticyclonic mesovortices decline. However, all cyclonic mesovortices do not produce tornadoes, which appear with a sudden increase of low-level vorticity. Nowadays, this process remains not utterly understood. A plausible explaination often suggested to characterize bow echo tornadoes as well as supercell ones is the transport of vorticity from the atmospheric layer between 1 and 3 km to the surface by strong downdrafts.

The commonly mentioned theory to explain mesovortices genesis in QLCS is described in Trapp and Weisman (2003). They consider that contrary to supercell cases where mechanisms leading to the vertical vorticity tilting are ascribable to updrafts, in bow echoes, this role is played by downdrafts at the leading edge of the cold pool. A synthetic scheme of mechanisms involved in mesovortices genesis is displayed in figure 1.6. Other studies indorse this downdraft theory. Particularly, Wakimoto et al. (2006) attribute mesovortices couplet formation to the titling of horizintal vortex lines by mechanically forced downdraft in the gust front. Wheatley and Trapp (2008) identify precipitation-induced downdrafts as the mechanism to tilt horizontal vorticity.

However, the up-to-date investigations of Atkins and St. Laurent (2009-b) lead to the conclusion that there may be several processes that produce mesovortices within bow echoes. Indeed, they point out in a quasi-idealized numerical simulation a mesovortices couplet genesis by the upward tilting of cold pool vortex lines due to a localized updraft maximum. The conceptual model of this mechanism is displayed in figure 1.7. Such mesovortices couplet seems to appear in the early stages of a bow echo life cycle. With a meridianal orientation of a bow echo moving eastwards, cyclonic vertical vorticity is generated to the north of the updraft and anticyclonic

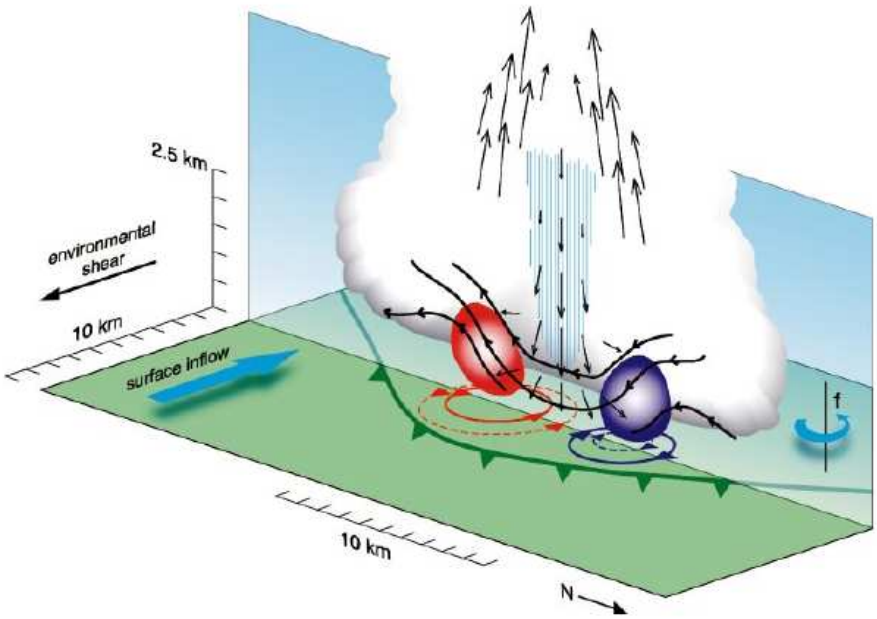

Figure 1.6: Schematic showing a proposed mechanism for low-level mesovortices genesis by downdraft within a QLCS. The green barbed line indicates the gust front, vectors are of air motion in the vertical plane, blue hatching depicts rain core, bold black lines are vortex lines in the vertical plane, and red (purple) areas indicate positive (negative) vertical vorticity in the vertical plane. Vortex lines are tilted vertically by the downdraft, resulting in a surface vortex couplet (red is cyclonic vortex; purple is anticyclonic vortex). The future state of the vortex couplet, which results in part from the stretching of planetary vorticity (f), is shown by the dashed red and purple circles. From Trapp and Weisman, (2003).

vorticity to the south. The localized updraft maximum is a consequence of a convective-scale downdraft within the outflow that locally accelerates the gust front outward. They also document the genesis of single cyclonic mesovortices which, on the opposite, affects all the stages of bow echoes life cycle. This genesis mechanism considers that the parcels descending within the downdraft acquires horizontal vorticity which is subsequently tilted by the updraft along the gust front. It is the same mechanism which leads to mesovortices in supercell thunderstorms (Rotunno and Klemp, 1985). When the shear magnitude presents moderate values, couplets of mesovortices are more frequently observed, whereas single cyclonic mesovortices prevail as the shear increases.

The next chapters analyse the case of 4^{th} October 2007, and allows to compare all the theories above mentionned with an observed case of squall line.

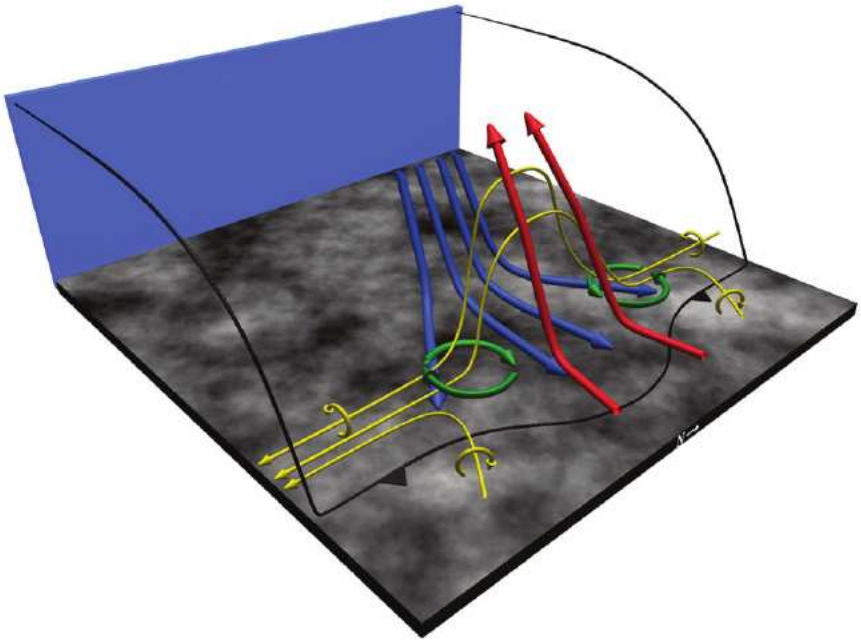

Figure 1.7: Schematic showing a proposed mechanism for low-level mesovortices genesis by updraft within a QLCS. Vortex lines (yellow), inflow (blue) and updrafts (red) are depicted. The thick green arrows represent the mesovortices. From Atkins and St. Laurent, (2009-b).

Chapter 2

Case description of the severe thunderstorm of 4^{th} October 2007

2.1 The event[1]

In the afternoon of 4^{th} October 2007, an exceptional thunderstorm crossed the island of Mallorca. A squall line entered the island from the south and moved northwards at a speed of 80 $km.h^{-1}$, accompanied with violent winds and torrential rain. Some videos of the event and the analysis of damages prove the presence of at least one tornado embedded in the system, later characterized by an F2-F3 intensity on Fujita scale. The city of Palma de Mallorca, and especially its industrial suburbs at the north, were the most affected areas and knew huge damages. Palma saw unprecedented traffic perturbations due to exceptional rain and wind intensities. Winds tore down hundreds of trees, traffic signs and lights, affecting road connections in the centre and north of the island. Some streets of Palma were flooded with more than 50 cm of water in places. This storm brought about 200 injured and even one fatality. Moreover, economic losses were huge, assessed to several tens of M€, only in Palma industrial area.

Let us see what were operational predictions for this event. On this day, INM[2] operational forecasters had been placed Balearic Islands in a yellow level of alert for rainfall, that is to say that it was expected to reach 20 mm in an hour. Just before the arrival of the MCS on Mallorca, helped by remote sensing data, they raised the alert at orange level for heavy precipitation, corresponding to 40 mm in an hour, and also broadcast an orange alert for storm. The INM commented that it was impossible to aware people before, as numerical models used did not allow a precise forecast for this kind of events.

2.2 Some observations

2.2.1 Ground observations

Before arriving over Mallorca, the squall line affected Ibiza at 14 UTC where gusts reached 80 $km.h^{-1}$. One hour later, the sky become utterly dark above Palma bay, as the system was progressing. Data registered in Mallorca during this afternoon indicate that rain exceed 40 mm during this severe event. The observatory of Palma recorded gusts reaching 109 $km.h^{-1}$ and the rain gauge measured 17.7 mm in only 10 minutes. Furthermore, this storm produced small-sized hailstones. The electric activity was also exceptional as the INM recorded 160 bolts of lightning in only 10 minutes.

[1] Event descriptions are partly based on a previous observational study of the case (Ramis et al. 2009)
[2] INM: Instituto Nacional de Meteorología, Spanish weather institute

The temperature graph of Santa Ponça in figure 2.1-a, city nearby Palma, shows a fall of 8 degrees with the passage of the MCS, which began one hour before the rain due to pre-squall clouds shrouding the sky, and which deepened sharply later, as a consequence of rain evaporation when the storm arrived. The pressure evolution during this day at Santa Ponça (figure 2.1-b), like in other Balearic weather stations, shows the signature of a pre-squall mesolow just before the arrival of heavy rain, followed by a mesohigh and then a wake low when the squall line was moving away. This kind of evolution matches with what was described in previous cases of observed squall lines (Ramis et al. 1999). This pressure chart also indicates high frequency pressure oscillations before the event, responsible of atmospherically forced seiches (quick sea level oscillations) at Ciutadella harbor in Menorca. These observations confirm the ocurrence of high-amplitude gravity waves over the western Mediterranean in the morning of 4^{th} October 2007. In addition, rainfall registered in Santa Ponça indicates the brevity and the strong intensity of rain associated with the squall line.

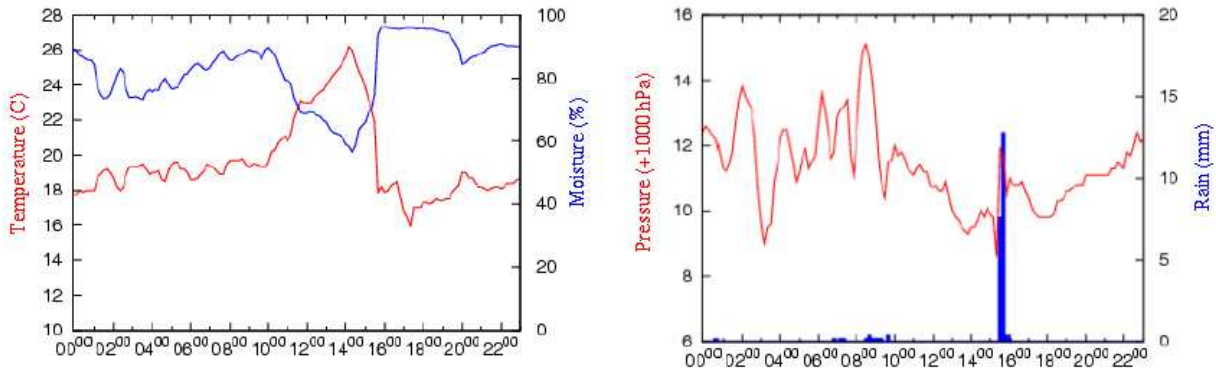

(a) (b)

Figure 2.1: Observations at Santa Ponça weather station on 4^{th} October 2007 : (a) temperature and relative humidity, (b) pressure and rainfall.

2.2.2 Radar and satellite data

Data from satellites and radars display more information about this storm, which initiated offshore of Murcia, at 06 UTC. It is interesting to note that during the night and the morning, two previous MCS evolved northeastwards over the sea. After the triggering of the third MCS, the thunderstorm stayed almost stationary from 7 to 10 UTC and HRV[3] pictures (figure 2.2-a) testify of a V-shaped structure of the thunderstorm. Later, this system began to progress slowly eastwards during two hours, before acquiring a faster northeastwards movement whereas a linear structure was forming in its south part. Even if it was located at the limit of the radar of Valencia, it can be inferred from lightning bolts that the squall line of about 60 km length had its more intense activity approching the bay of Palma at 15 UTC. In the time sequence shown in figure 2.3, the progressive transformation of the V-shaped stucture into a squall line is clearly identifiable. At this time, the overshooting cloud tops were impressive, reaching 16 km of height, a very unusual feature at our latitudes. The resulting upper-troposphere perturbation is reflected by gravity waves clearly visible in HRV pictures (figure 2.2-b). Associated with this squall line, a widespread stratiform part further west was shrouding the Balearic channel.

[3]HRV: High Resolution Visible

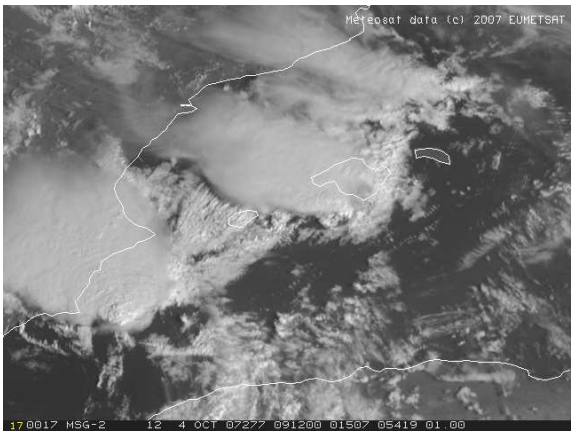

(a)

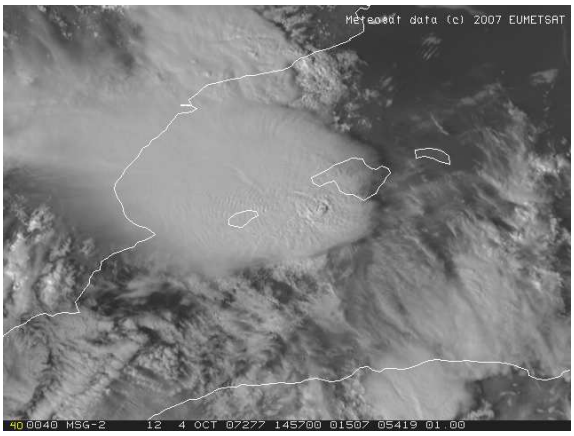

(b)

Figure 2.2: HRV images of the event at(a) 9h15 UTC and (b) 15 UTC.

2.3 Analysis of synoptic patterns

2.3.1 Synoptic charts

In the upper levels, the synoptic situation was charactarized by an upper-level trough over mainland Spain associated with cold air aloft which promoted the potential instability (figure 2.4-a). This cut-off enhances a southwesterly flow at mid and upper tropospheric levels which results in a divergent jet aloft streching from North-Africa to Balearic Islands. The synoptic scenario at low-levels was dominated by a dynamic low centered over the Sahara in the morning, moving as the hours go by towards Balearic archipelago along the edge of the upper-level perturbation. This low pressure area induces an easterly flow over southern Mediterranean sea. As shown by ARPEGE[4] analysis in figure 2.4-b, a strong baroclinic area along the Spanish coast separated a tongue of African warm air, located over the sea, from drier and colder air over Spain. At the south of Balearic Islands this boundary can be qualified as a cold front moving slowly eastwards. More to the north, it matches to a warm front progressing westwards. This baroclinic boundary also corresponds to a convergence line of low-level winds and is characterized by a strong advection of moisture. ARPEGE and ECMWF[5] analyses indicate that the cold front structure looks like a katafront, with a dry layer at mid levels above the western part of the warm tongue.

Therefore, the synoptic environment is characterized by a well defined quasi-geostrophic forcing favourable to upwards motions. Moreover, as usual in early fall, sea surface temperature was high in this area, as testified by the $23°C$ measured offshore of Balearic islands. Consequently, a strong evaporation provides a large amount of moisture at low-levels. This kind of scenario increases convective instability inducing deep convection with sometimes flash-flood near Mediterranean coasts of Spain and France.

The presence of gravity waves has to be connected with synoptic patterns present on 4^{th} October 2007 favouring their genesis. First, a diffluent region aloft is bounded by a ridge axis to the east and a trough axis to the west. Then, their presence has to be related with a southwesterly upper-level jet streak propagating out of the mean trough and toward the downstream ridge axis. This configuration produces a divergent ageostrophic flow which is in an unbalanced state. A warm front in low-levels is also an important feature favouring gravity waves development. Gravity waves are a well known mechanism often efficient to initiate convection.

[4]ARPEGE: Action de Recherche pour la Petite Echelle et la Grande Echelle, French global model
[5]ECMWF: European Centre for Medium-Range Weather Forecasts

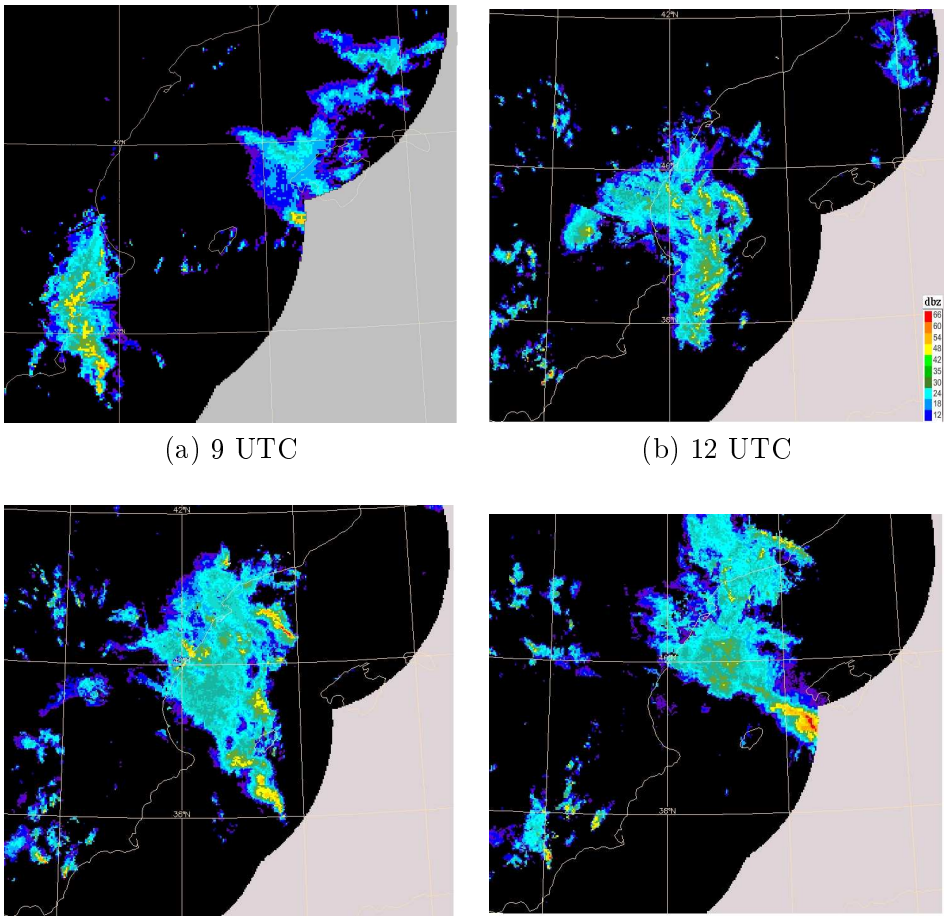

(a) 9 UTC (b) 12 UTC

(c) 13h30 UTC (d) 15 UTC

Figure 2.3: Radar reflectivities from 9 UTC to 15 UTC.

2.3.2 Vertical profile

The sounding from Murcia at 00 UTC presented in figure 2.5-a, proximity sounding of the onset of the thunderstorm, gives a good idea of the initialization environnement. The temperature profile is lightly unsettled with a CAPE value at 62 $J.kg^{-1}$. However, it can be assumed that the CAPE value is higher offshore of Murcia, as the surface cooling during the night is weaker over the sea. This profile is dry enough, particularly within the layer between 600 and 450 hPa. This confirms the katafont theory above-mentioned. The unidirectional shear below 700 hPa is remarquable and is supportive to explain the initial multicellular V-shaped structure of the thunderstorm.

The analysis of the sounding from Palma at 12 UTC displayed in figure 2.5-b indicates some interesting features which contribute to explain the squall line organization. Even if the instability is not very pronounced at this time with a CAPE at 38 $J.kg^{-1}$, a dry layer between 950 and 700 hPa is a classical feature of pre-squall line environments and results in the creation of substantial convective inibition energy ($CIN = 355\ J.kg^{-1}$) at low-levels. In addition, a strong southwesterly shear of about 20 $m.s^{-1}$ in the three first kilometers of the troposphere is also present over this area.

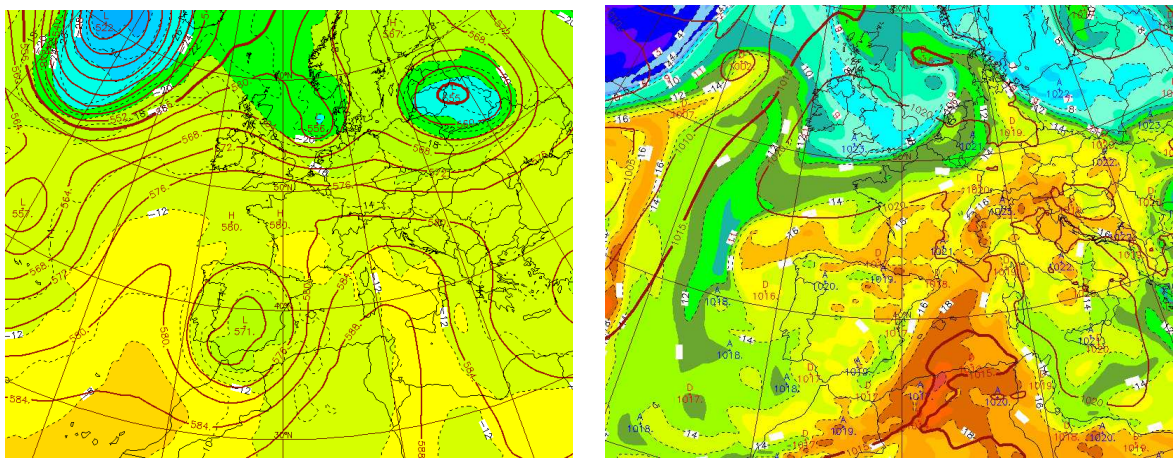

(a) (b)

Figure 2.4: Synoptic patterns: (a) ARPEGE analysis at 12 UTC of geopotential and temperature at 500 hPa, (b) mean sea level pressure and wet bulb potential temperature at 850 hPa.

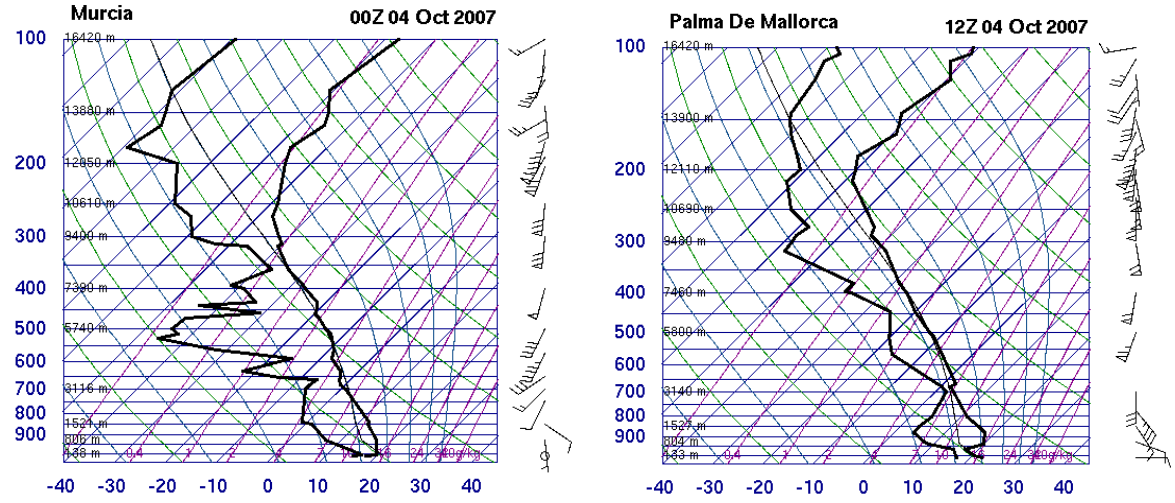

(a) (b)

Figure 2.5: Soundings from: (a) Murcia at 00UTC, and (b)Palma at 12 UTC, from University of Wyoming.

2.3.3 Summary of meteorological conditions favourable to the squall line formation

On 4^{th} October 2007, several specific meteorological patterns were favourable to deep convection and others were indicative of a squall line organization. First, at low-levels a baroclinic area was streching over the western Mediterranean with a strong warm and moist easterly advection. At mid-levels, a low was centered over Spain inducing a southwesterly divergent flow in the same area, which was associated with a strong PV anomaly. The dry layer capping the warm one is also a crucial element to enhance deep convection since it increases the rainfall evaporation rate, therefore the cooling responsible of stronger downdrafts. In spite of the fact that there was a strong inversion at low-levels, in Balearic Islands area, some elements were able to release instability by breaking the dry layer. First an upper-level trough was moving northeastwards in the morning along the baroclinic area producing dynamic lifting. Then, the front is characterized by a severe convergence of low-level winds. Next, the presence of earlier deep convection may have led perturbed areas of surface pressure and winds. At least, gravity waves associated with

the upper-level jet streak and the warm air at low-levels, are also able to trigger convection. Although it is intricate to identifiy which one of these factors prevails, their combination may had enabled a more efficient triggering.

Even if most of the time it is difficult to distinguish development of squall line from development of an isolated storm, here some clues can indicate an important likelihood to see preferentially this kind of structure among other MCS. First, the presence of a front which can be identified as a katafront seems to be favourable to squall line development. In addition, the strong shear of horizontal wind present along the coastal area is a crucial pattern for squall lines sustainment. In the next chapters, we will investigate if numerical models used with high resolution are able to simulate the squall line of 4^{th} October 2007 over western Mediterranean.

Chapter 3

Numerical simulations with three fine resolution models

3.1 Models descriptions and parameterizations

Simulations are performed with three different fine resolution models to test their ability to capture the squall line event of 4^{th} October 2007. Thus, this study includes results given by the French research model Méso-NH, and by two American models, MM5 and WRF. Although domains and mesh configurations are akin, dynamical and physical schemes have been developed only for their respective models. Configurations chosen to run these models are thought to be optimised to simulate deep convection events, and are described in the following paragraphs.

3.1.1 Méso-NH

Méso-NH is a French 3D non-hydrostatic model (Lafore et al. 1998) in which the prognostic variables are the following: three dimensional wind components, potential temperature, turbulent kinetic energy, mixing ratio of vapour and of five hydrometeors classes. Its temporal scheme is hybrid using a 4^{th} order and centered scheme for momentum, and a PPM[1] advection scheme (Colella and Woodward, 1984) for scalar variables. The model of cloud microphysics is a bulk scheme (Caniaux et al. 1994; Pinty and Jabouille, 1998) using three ice categories (primary ice, snow and graupel) combined with a Kessler scheme for warm process separating cloud water from rainwater. Contrary to other mesoscales models, Méso-NH is based on the anelastic approximation, which means that acoustic waves are filtered. Méso-NH can be run with several nested grids in two-way interactive mode (Clark and Farely, 1984; Stein et al. 2000). In several experiments, two grids will be used to simulate the event. For the high resolution grid, no convection parameterization is used, whereas in the coarser domain, a deep convection scheme is activated. The turbulence parameterization is founded on a 1.5 order closure (Cuxart et al. 2000) with the Bougeault and Lacarrère mixing length (1989). For the coarser grid, only vertical turbulent fluxes are taken into account, whereas in the fine grid all turbulent fluxes are computed.

In each simulation with the three models, the fine grid domain called hereafter D_1 will be the approximately the same, a square of about $700 * 700\ km^2$ centered in the west of Mallorca, and streching from North Africa to south of France. As Méso-NH is used with grid-nesting, the location of coarser grid depends on the boundary conditions. Indeed, with global analyses as those of ECMWF or ARPEGE, the coarser area (D_2) can be placed more south than with ALADIN[2] analyses (D_3), as its domain is limited. All these domains are displayed in figure 3.1-a. The simulation on the fine grid is performed with a 2.4 km grid length and the one of the coarser

[1] PPM: Piecewise Parabolic Method

[2] ALADIN: Aire Limitée Adaptation dynamique Développement InterNational

domain is four times larger, that is to say 9.6 km, the ALADIN resolution. On the vertical, 40 levels are used, spaced with 75 m near the ground and up to 900 m in the model upper layers.

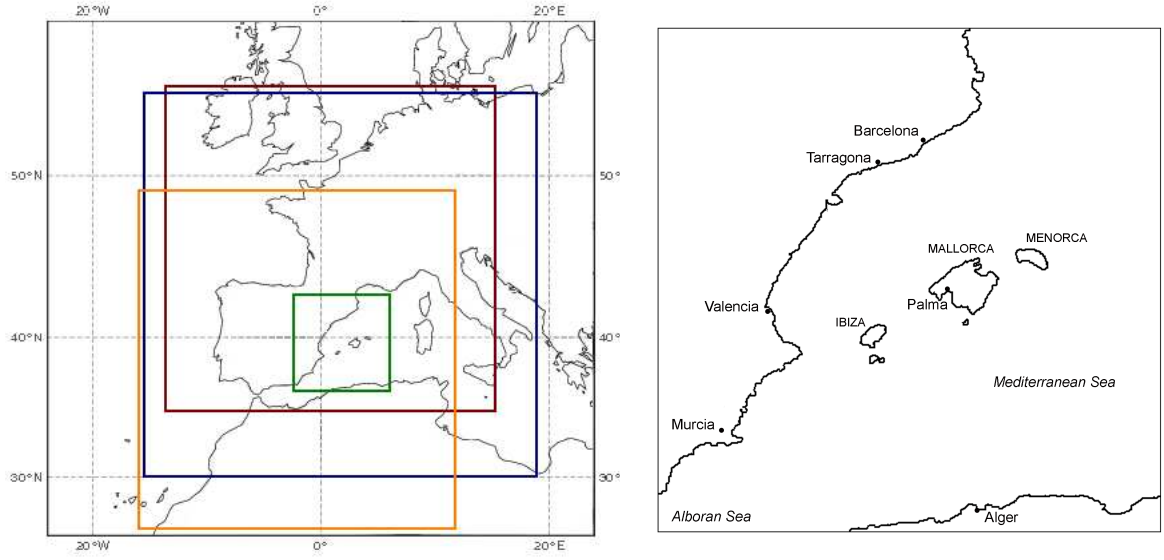

(a) (b)

Figure 3.1: (a): Domains used for simulations, high resolution domain in green (D_1), parent domain for Méso-NH fed with ARPEGE and ECMWF (D_2) in blue, and with ALADIN (D_3) in brown, parent domain for WRF fed with ECMWF in orange (D_1); (b): geographic references in D_1.

3.1.2 WRF

The Weather Research and Forecasting (WRF) model is a mesocale numerical weather prediction system, mainly developed by the NCAR[3] and the NCEP[4], designed to be used in both operational forecasting and atmospheric research. It is based on fully compressible equations and uses a 5^{th} order advection scheme on the horizontal and a 3^{rd} order scheme on the vertical, both for scalar and momentum variables. To study the squall line case, the non-hydrostatic option is chosen and several physical parameterizations are used. First, owning to the fine resolution of the simulations, no deep convection parameterization is employed. The microphysical scheme, named WSM-6 is also based on 6 hydrometeors species including graupel (Hong and Lim, 2006). Flux computation in the surface layer follows the Monin-Obukhov (1954) similarity theory in conjunction with the Carlson-Boland (1978) viscous sublayer.

WRF simulations are also performed with and without grid nesting, on nearly the same domain as D_1 with a mesh of 2 km. In nested experiments, also performed in two way (Gill et al. 2004), the parent model is run with a resolution of 10 km on domain D_4 more south than MNH domains in order to later study Atlas influence. When only one grid is used, boundary conditions of the fine domain are directly provided by ECMWF analyses, available every 6 hours. These experiments are computed with 35 vertical sigma levels refined in the planetary boundary layer, where the first levels are spaced by 40 m.

[3]NCAR: National Center for Atmospheric Research
[4]NCEP: National Centers for Environmental Prediction

3.1.3 MM5

The PSU[5]/NCAR mesoscale model known as MM5 is a limited-area model based upon the set of primitive equations for a fully compressible and nonhydrostatic atmosphere, and designed to simulate or predict mesoscale atmospheric circulations. Its temporal scheme is simpler than those of both other models, as it uses a 2^{nd} order advection scheme. Physical parameterizations available are also different from those used in previous models, and the following choices are those used for the daily "operational" run of MM5 performed at the UIB [6]. The microphysical scheme called Reisner 2 has the particularity to add a supercooled water specie to the six others above-mentioned (Reisner et al. 1998). In the planetary boundary layer, the Hong-Pan scheme (1996) adapted to high resolution predictions is applied. The scheme of deep convection is not activated as these processes are thought to be resolved with the 2 km resolution used. Experiments are performed on the domain D_1 with 30 unequally spaced sigma levels on the vertical, whose interval ranges from 40 m near the ground to about 2 km in upper layers.

MM5 allows to realize four-dimensional data assimilation using the Newtonian-relaxation technique known as nudging. One way to introduce observations in MM5 forecasts is to perform station nudging. This method resorts to relaxation terms added to the prognostic equations for wind, temperature, and water vapor. Theses terms are based on the model error at observational stations and are such as to reduce this error. Each observation can be completed by three features, a radius of influence, a time window and a nudging factor to determine respectively where, when and how much it affects the model solution. If a model grid point is located within the radius of influence of several observations, their contributions will be weighted according to their distance. The nudging factor G_α for each parameter α is based on scaling arguments and must satisfy the numerical stability criterion $G_\alpha \leq \frac{1}{\Delta t}$. Typical values of G_α range from 10^{-4} s^{-1} to 10^{-3} s^{-1}. A large value of G_α will force the model state strongly towards observations.

3.2 Experiments

3.2.1 First experiments

Several experiments are made with the three mesoscale models and their characteristics are summarized in table 3.1. In order to test the sensitivity to initial conditions, different analyses are available. Simulation are carried out in a case study configuration, that is to say with analyses which provide boundary conditions. The impact of models physics and dynamics will be determined with simulations run with the same initial conditions. Some experiments computed with an without grid nesting will be compared to understand the influence of boundary conditions. All these experiments begin on 4^{th} October 2007 at 00 UTC and extend up to 24 hours. The time step chosen to compute each prognostic variable in the domain D_1 is rather low, between 4 and 8 s depending on the experiments, so as to guarantee stability conditions. The main contraint is caused by vertical velocities which are supposed to be very important in such squall line.

3.2.2 Complementary investigations

At the end of the analysis of this ensemble of simulations, other experiments will be performed guided by the conclusions derived from first set of simulations.

[5]PSU: Pennsylvania State University
[6]UIB: Universitat de les Illes Balears

n° exp.	name	model	initial/boudary conditions	resolution	nesting
1	MNHcep	Méso-NH	ECMWF analyses	2.4 km	no
2	MNHarp	Méso-NH	ARPEGE analyses	2.4 km	no
3	MNHala	Méso-NH	ALADIN analyses	2.4 km	no
4	MNHcepN	Méso-NH	ECMWF analyses	2.4 km	yes
5	MNHarpN	Méso-NH	ARPEGE analyses	2.4 km	yes
6	MNHalaN	Méso-NH	ALADIN analyses	2.4 km	yes
7	WRFcep	WRF	ECMWF analyses	2 km	no
8	WRFcepN	WRF	ECMWF analyses	2 km	yes
9	MM5cep	MM5	ECMWF analyses	2 km	no

Table 3.1: Simulations characteristics

3.2.2.1 Assimilation of subjective pseudo-observations with nudging

First, thanks to MM5, an attempt to improve MM5cep simulation using observational nudging will be carried out. This nudged experiment called MM5nud is run with the same configuration than MM5cep, and the only difference consists in adding observations. As this subjective method is wholly dependent on previous results, pseudo-observations assimilated will be described in next chapter, in section 4.3.

3.2.2.2 Planetary boundary layer scheme influence

It would be interesting to test if simulations are sensitive to physical schemes used by numerical models. More precisely, in this squall line event, PBL[7] parameterizations can be relevant to trigger deep convection, through their representation of low-level environment. Therefore, this study focuses on the comparison of two PBL schemes commonly used with MM5, the Hong-Pan scheme also called MRF[8] and the Mellor-Yamada scheme (ETA) as used in the Eta model (Janjić, 1994). These two schemes mainly differ by their representation of turbulence and following paragraphs present an overview of their features. Both first order (MRF) and TKE[9] based closure (ETA) schemes are based on the concept of a mixing length, and require the computation of an eddy coefficient (K). The reference simulation performed with MRF (MM5cep) was previously described and the other run with ETA PBL scheme is called MM5pbl.

- **MRF scheme**

This scheme has been developed to be used in NCEP operational forecasts with MRF model. It is a first-order scheme in which the gradients of horizontally averaged, first-order flow variables (such as wind and temperature) are used to predict the eddy exchange coefficients. It resorts to a non-local vertical diffusion scheme to represent mixing in the boundary layer, taking into account larger turbulent eddies, that is thought to lead to a better representation of convective well-mixed layers. Moreover, it has the particularity to employ the counter-gradient flux term for potential temperatures. The scheme uses Richardson number and velocity scaling criteria to diagnose the PBL depth and then calculates mixing coefficients K for vertical diffusion according to a similar profile over the PBL depth. This diagnosis is carried out in the same way for convective, neutral, and stable PBL, even if the profile of eddy exchange coefficients may differ in each case. Parameterizations used are described in Hong and Pan, 1996.

[7]PBL: Planetary Boundary Layer
[8]MRF: Medium Range Forcast model
[9]TKE: Turbulent Kinetic Energy

- **ETA scheme**

The Eta PBL parameterization in MM5 is based on the implementation of Mellor and Yamada (1974) theory in the NCEP Eta model (Janjić, 1994). It is a local, one-and-a-half order closure PBL scheme with a prognostic equation for TKE. It resorts to local forecast of vertical mixing of horizontal wind, potential temperature, and mixing ratio to diagnose PBL depth. For this local type of closure, the turbulent fluxes of momentum, heat, and humidity at a point are determined from mean atmospheric variables and their gradients at that point, using turbulence closure at 1.5 order. The scheme incorporates parameterizations to take into account effects of anisotropy but specifically carries a prognostic equation for TKE and uses such TKE values to calculate eddy exchange coefficients. Under unstable conditions, certain constraints are imposed to avoid the development of too-large K coefficients. In general PBL growth is slower with local and TKE schemes because of the slower diffusion and since the predicted TKE does not take into account a deeper convective boundary layer.

3.2.2.3 Influence of the Atlas mountains

Even if the squall line triggering and evolution occured over the sea, the proximity with the mountainous African continent leads to the hypothesis of an indirect influence of Atlas mountains range in the initial convective location. Indeed, the presence of an orography higher than 1000 m just south of the area of interest is thought to deflect the southerly flow mentioned in section 2.3.1. In order to better understand how it affects weather patterns, a drastic solution is to remove Atlas range. To be rigorous, this change has to be made on a domain including the whole mountain chain. The simulation WRFcepN offers this possibility as the parent model run on D_4 contains all North Africa. Therefore, a sensitivity experiment called WRFatlas is performed with WRF forced by ECMWF analyses with the same parameterizations than WRFcepN, but with the African orography removed in both D_1 and D_4 domains. All the other ground features remain unchanged.

Chapter 4

Results

4.1 Initial conditions differences

An interesting way to assess experiments representativity is to analyse initial condition correctness. This comparative approach is commonly used by forecasters to characterize prediction uncertainties and to chose a reference scenario. In this study, initial conditions used are provided by coarse analyses from ECMWF, ARPEGE and ALADIN and their differences should have an impact on the squall line modeling. Although weather conditions are quite similar aloft between the three analyses, an overview of low-level patterns of each analysis at 00 UTC in figure 4.1 indicates some interesting elements which are thought to be reflected in model evolutions. First, as concerns winds at 925 hPa, ARPEGE and ECMWF charts are quite close with an easterly flow going along the African coastline. On the ALADIN analysis, this flow is stronger and presents a more southeasterly direction veering strongly over the south of Balearic Islands, along a thermal boundary. Thus a convergence line is already present in ALADIN analysis within the low-level warm and moist air mass. In the case of ALADIN experiments, it is noteworthy that the interest area is not so far from the model south limit, probably characterized by lateral effects. However, the problematical issue is the fact that there is not any observation that support more ARPEGE or ECMWF wind chart than the ALADIN one, since differences are mainly located over the Mediterranean sea.

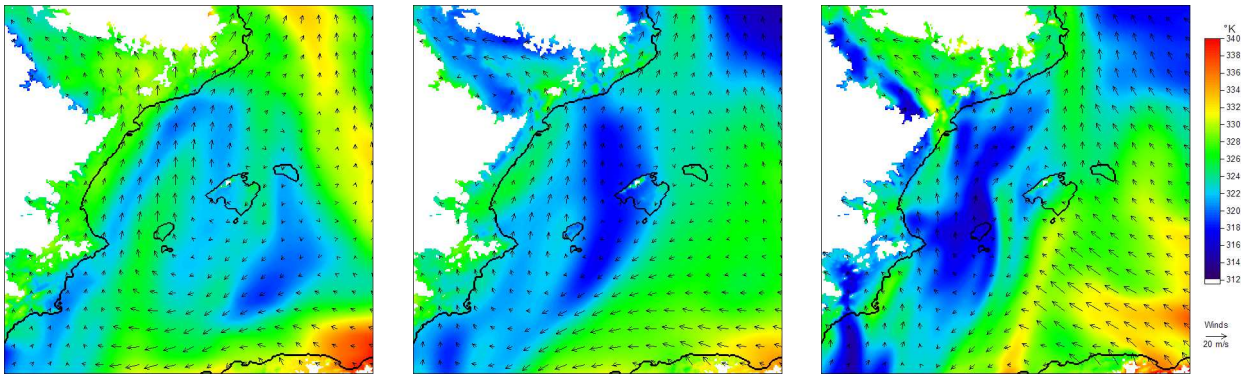

ECMWF (a) ARPEGE (b) ALADIN (c)

Figure 4.1: Initial conditions at 925 hPa: equivalent potential temperature and winds from (a) ECMWF, (b) ARPEGE and (c) ALADIN.

Although wind charts between AEPEGE and ECMWF analyses are rather similar, those of EPT[1] present more significant differences. Indeed, at 00 UTC a thermal front is already visible

[1]EPT: equivalent potential temperature

in figure 4.1-b whereas ECMWF chart presents more intricate features. It is interesting to note that EPT in ECMWF analysis is higher along the Spanish coast. Consequently, this area will be more favourable to convective developments. In addition, with ECMWF initial conditions, the main baroclinic boundary is located to the southeast of the domain, whereas a tongue of warm air stretches near the coast. In this case again, it is difficult to know which one of the initial conditions datasets abides the best analyses between ARPEGE and ECMWF. Nevertheless, the area of effective triggering of the squall line is characterized by quite similar thermal features in both analyses. Finally, the lack of observations over the Mediterranean sea seems to be the main reason for such differences between initial analyses. Numerical simulations are expected to provide elements to precise the basic role exerted by initial conditions.

4.2 Experiments analysis

4.2.1 Temporal evolution

The main difficulty to discuss the quality of an experiment is to compare the results to the few surface observations available since the event occured over the sea. In addition, coastal observations indicate a weak and intricate low-level flow, associated with a complex distribution of sea level pressure. Consequently, a crucial tool to assess the accuracy of experiments will be remote sensing data like radar reflectivities and satellite imagery (figures 2.2 and 2.3). So as to present characteristics of each experiment, a mosaic of reflectivities at 800 hPa and low-level winds at 925 hPa for the 9 experiments mentioned in table 3.1 is displayed in figures 4.2, 4.3 and 4.4 corresponding at 9, 12 and 15 UTC respectively. Results are described for each one in the following paragraphs.

Méso-NH with ECMWF analyses (MNHcep): In this experiment, a convective cell (A1) forms offshore of Murcia between 7 and 8 UTC in a good spatial correspondence with satellite observations (not shown). On the opposite, at 9 UTC other convective systems apparent along the coast (A0) affected in reality Balearic Islands. The triggering of the cell offshore of Murcia is a response to the convergence of low-level winds, between a well established easterly flow and an area of very weak winds associated with a low centered over Murcia. This area is especially favourable to the triggering as it is characterized by a warm air tongue at low-levels and a pool of cold air aloft. Nevertheless, even if the cell A1 is born in good spatiotemporal conditions, it does not stay at the same place during few hours as seen in observations. It begins to move northeastwards three hours earlier and affects Mallorca at 13 UTC whereas it actually occured at 15h30 UTC. In spite of the lack of initial stationarity, the positive aspect of this experiment is that later, Méso-NH succeeds in reproducing the squall line, well fed by a perpendicular low-level moist flow. Reflectivities computed in this experiment are very similar to those observed (figure 2.3-d) although they present a three hours lag.

Méso-NH with ARPEGE analyses (MNHarp): This experiment presents also a well defined convergence line early in the morning allowing the triggering of two main cells at 8 UTC (B1 and B2). At 9 UTC the situation is rather correctly represented by the model which also succeeds in reproducing mature thunderstorms over Balearic Islands (B0). The initial stationarity is captured well enough, with the persistence of wind characteristics from 7 to 9 UTC in the triggering area in the whole PBL. However, the two initial thunderstorms B1 and B2 do not merge later to form a more powerful system, but evolve separately. Thanks to remote sensing data, it is proved that several systems were present in the MCS and more precisely other weaker linear organizations were located to the north. But here, the first cell B1 is more developed and able to generate an outflow boundary which seems to prevent the good evolution of the second

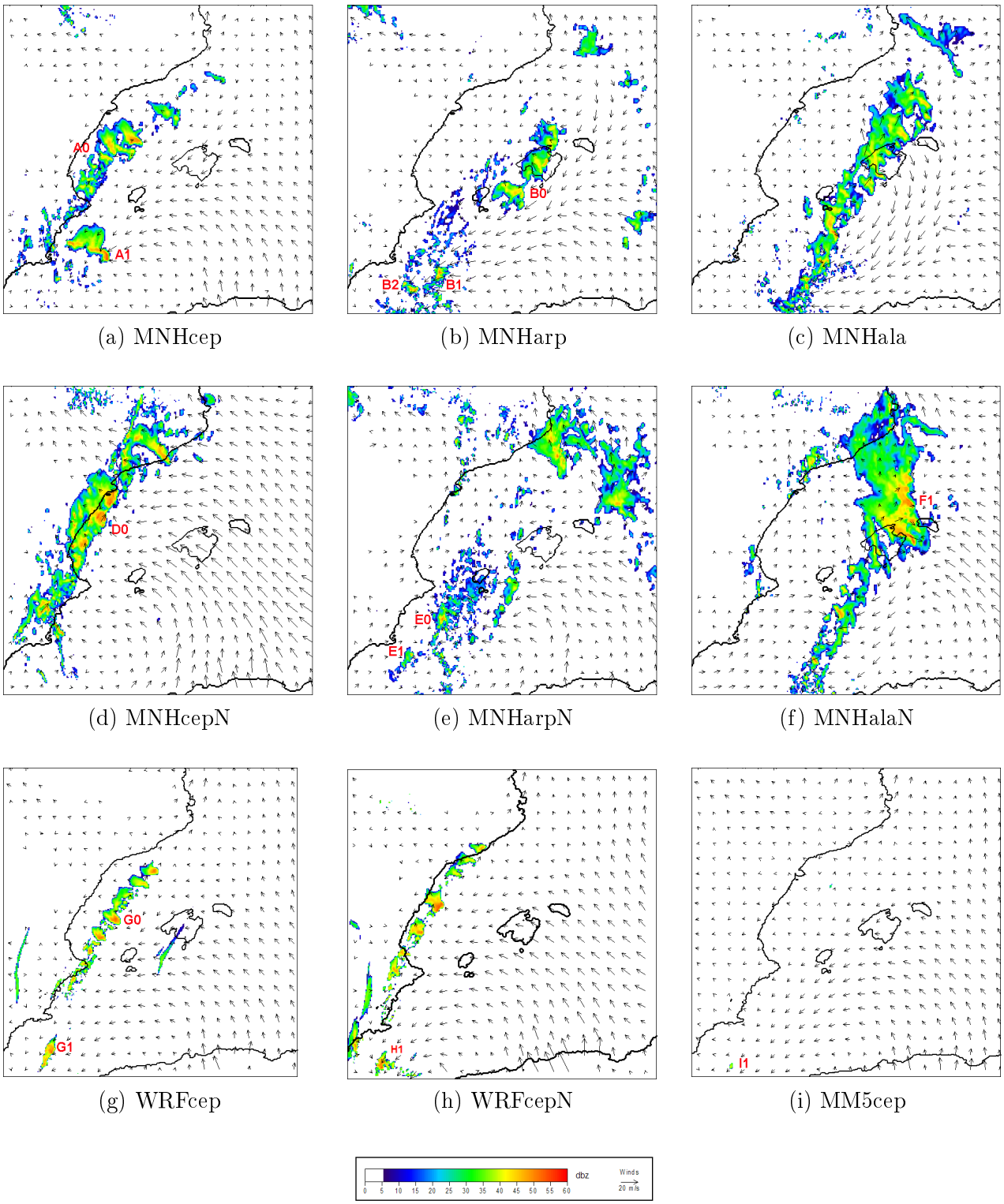

(a) MNHcep (b) MNHarp (c) MNHala

(d) MNHcepN (e) MNHarpN (f) MNHalaN

(g) WRFcep (h) WRFcepN (i) MM5cep

Figure 4.2: Results at 9 UTC, reflectivities at 800 hPa and winds at 925 hPa for table 3.1 simulations.

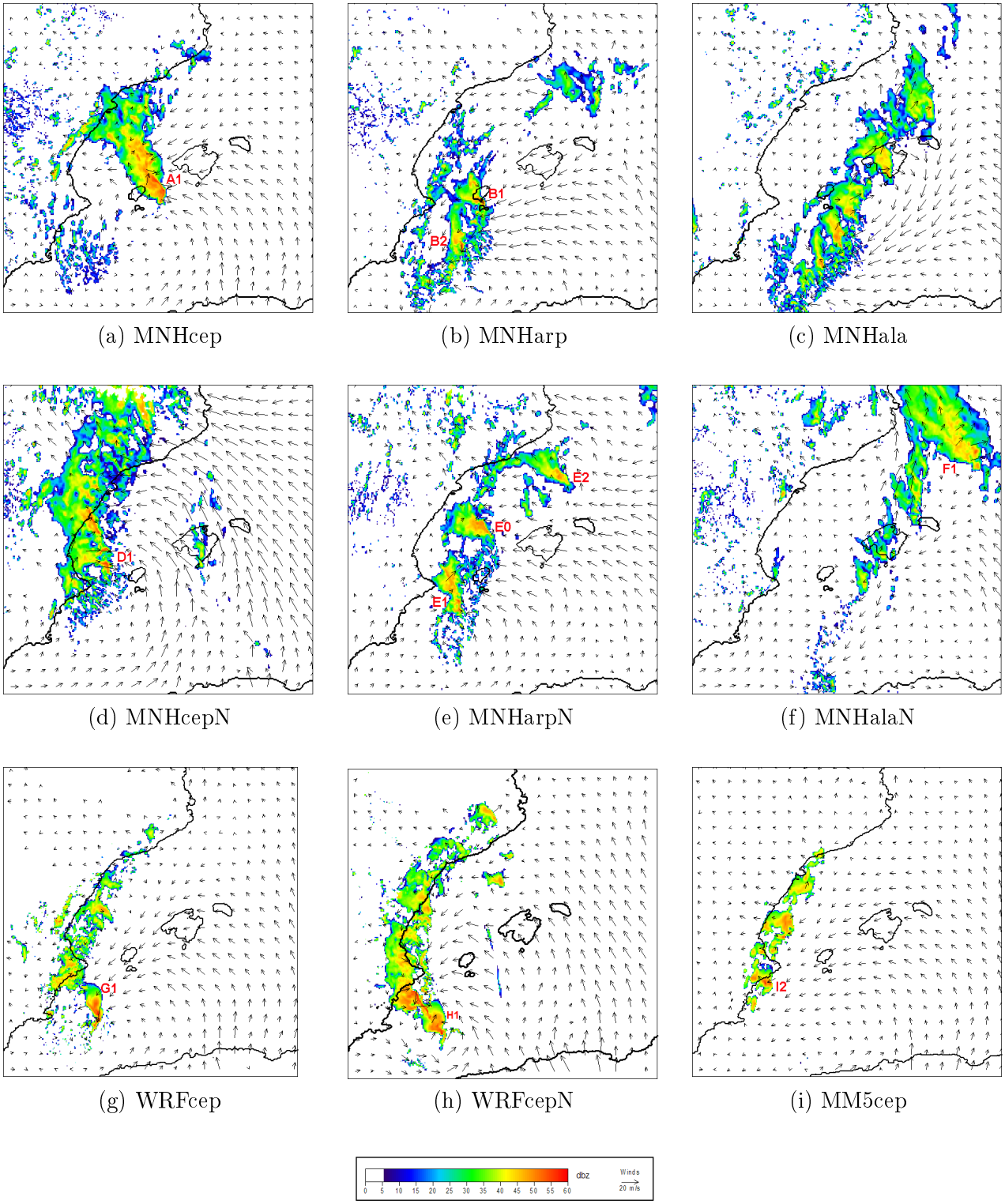

(a) MNHcep (b) MNHarp (c) MNHala

(d) MNHcepN (e) MNHarpN (f) MNHalaN

(g) WRFcep (h) WRFcepN (i) MM5cep

Figure 4.3: Results at 12 UTC, reflectivities at 800 hPa and winds at 925 hPa for table 3.1 simulations.

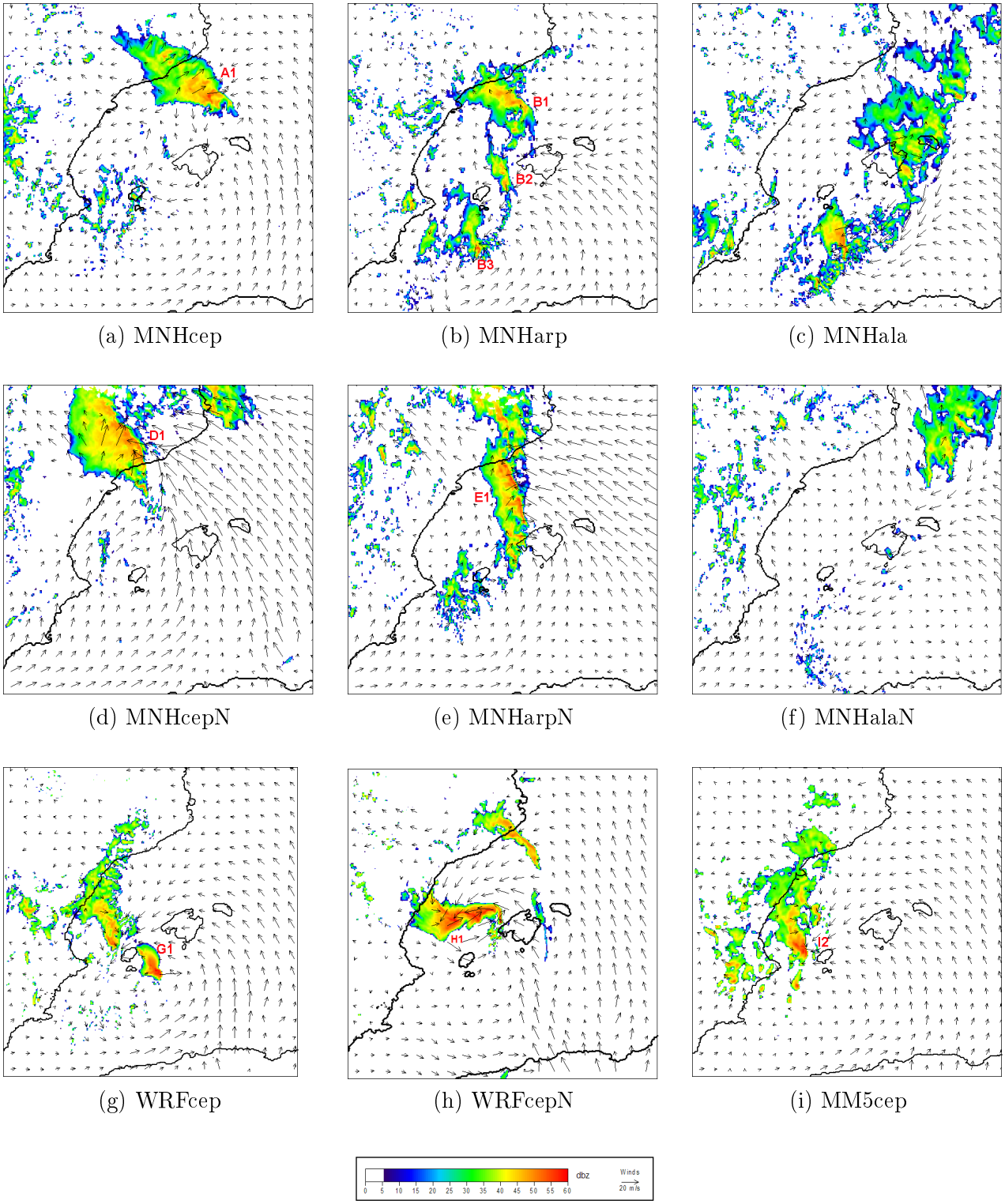

(a) MNHcep (b) MNHarp (c) MNHala

(d) MNHcepN (e) MNHarpN (f) MNHalaN

(g) WRFcep (h) WRFcepN (i) MM5cep

Figure 4.4: Results at 15 UTC, reflectivities at 800 hPa and winds at 925 hPa for table 3.1 simulations.

cell B2. Indeed, a perturbed divergent area avoids the easterly flow to feed the thunderstorm, which steadily weakens. In addition, a third system (B3), absent in the reality, is formed after the two previous ones and follows the same northeastwards evolution.

Méso-NH with ALADIN analyses (MNHala): This experiment is the only one which fails to create any squall line. Simulation beginning is characterized by a strong convergence line and a moist area over Balearic Islands. These features persist during the morning and several convective systems evolve along the convergence line all the day long but no one enough develops to reach the squall line stage. The low-level flow affecting the east of the domain presents a southeasterly direction which avoids the creation of a linear organization of cells.

Méso-NH with ECMWF analyses and grid nesting (MNHcepN): This experiment fails to trigger a cell offshore of Murcia, and creates a convergence line in the morning along the eastern coast of Spain whereas the flow is very weak and disorganized around the effective place of triggering. The linear area of rainfall in the morning (D0) is located too much to the west compared with real precipitating structures which happened over Balearic Islands. At sea level, the wind chart does not seem to be coherent with the few observations, particularly at 9 UTC where the northerly flow component over Balearic archipelago is not captured. A convective system presenting squall line features develops later to the north of Valencia (D1), where the strongest convergence is observed, and evolves along the Spanish coast. To sum up, this simulation is characterized by a spatial lag of the low pressure area at low-levels which seems to be located too northwestwards, avoiding convection triggering offshore of Murcia.

Méso-NH with ARPEGE analyses and grid nesting (MNHarpN): In this experiment, the triggering is rather correct, although it occurs slightly too southwards. At 9 UTC the convective cell E1 is rather well located but later, the model fails in reproducing the stage characterized by a slowly eastwards motion associated to the V-shaped structure. As a result, the evolution of this main cell happens to the west of the real zone. On the figure 4.3-e at 12 UTC, despite the light western lag, there is a good agreement with the observed radar reflectivites (figure 2.3-b), with two other short and linear convective systems (E0 and E2) along the Spanish coast. At this stage, the MCS has acquired a linear organization mainly favoured in its northern part due to the presence of the easterly strong low-level flow. At 15 UTC the squall line sweeps across the east of Mallorca with an excessive meridian orientation and a still more developed part to the north. On the whole, this simulation is characterized by a initial spatial lag which avoids a further correct evolution of the squall line.

Méso-NH with ALADIN analyses and grid nesting (MNHalaN): As in MNHala, from the first hours of the simulation Méso-NH creates a broad and facticious convective system over Balearic Islands associated with a neighbouring subsidence area and therefore divergence at sea level. Consequently this new feature interacts with the easterly flow to create a strong convergence line, streching from Mallorca to Algeria, that is to say in the warm side of the baroclinic area. Several thunderstorms develop along this convergence line and the main convective system (F1) crosses Mallorca between 8 and 9 UTC, before getting a linear organization around 10 UTC, when the MCS is really under the influence of the easterly flow. Therefore, this experiment presents incorrect flow features in the morning leading to a too early triggering and an evolution significantly far from reality.

WRF with ECMWF analyses (WRFcep): This experiment with WRF is the one which produces the best results, with good spatiotemporal features of the squall line. A more complete study of the squall line environment will be done with these results in section 4.2.2.1. Nevertheless, although this simulation succeeds in creating a short squall line crossing Mallorca at

16 UTC, its representation of the event is not entirely satisfactory. First, as described in other experiments with these analyses, earlier convection (G0) is misplaced from Balearic archipelago to the Spanish coast. Then, the triggering of the cell G1 which transforms later into the squall line takes place almost in the southwest edge of the domain due to a weak low-level convergence at 7 UTC, therefore with a lag greater than 100 km. In addition the model fails in reproducing initial stages of stationarity and slow eastwards movement, and the simulated squall line is rather characterized by a slowly and continuous northeastwards motion.

WRF with ECMWF analyses and grid nesting (WRFcepN): In this simulation the convective triggering of the cell H1 caused by a convergence line in the Alboran sea occurs around 9 UTC, that is to say slightly too late and too south. Wind magnitudes computed at the south of the Mediteranean basin seem very high and their veering around a pressure low offshore of Murcia is clearly visible. Then a linear organization forms after 11 UTC and acquires a high translational speed. However, strong winds over the sea drive the MCS too westwards and the line reaches only the western cape of Mallorca with a satisfactory zonal orientation. Remarks made on MNHcep triggering are also valid in this experiment. In addition, further evolution seems to be worse due to an overestimation of the steering winds.

MM5 with ECMWF analyses (MM5cep): With the MM5 model, low-level flow patterns do not manage to sustain a cell (I1) present around 8 UTC. At 9 UTC no precipitating system is apparent, even along the coast where convection only develops later, too westerwards as in other simulations fed with ECMWF analyses. The evolution of this simulation looks like the one described in the experiment MNHcepN. Indeed, a short squall line (I2) generated to the south of the coastal convection follows the Spanish seashore. Consequently, this system crosses the Mediterranean sea to the west of Mallorca with a inaccurate chronology. In this experiment, the lack of convergence at low-levels can be thought to be the reason for the imprecise triggering and consequently for the incorrect evolution of the squall line.

First conclusions

After completion of these experiments, some interesting conclusions can be already drawn. Analysing the differences between Méso-NH simulations, the role played by initial conditions seems to be relevant since results are farly different when ECMWF, ARPEGE, and especially ALADIN analyses are used. These distinct behaviours will be precised in section 4.2.3. Moreover, boundary conditions also influence the representation of the event, as inferred from simulations with and without grid nesting. Their impact exerts an important role on the triggering of the squall line and is latter discussed in section 4.2.4. Finally, dynamical and physical parameterizations of the three models available have also a strong influence on the modeling of this case, as shown by the different results obtained with ECMWF analyses. It will be very difficult to determine which parameterizations seem to be responsible for such distinct behaviours, since for example physical schemes are not interchangeable from one model to another. Section 4.2.5 will rather point out physical differences on meteorological patterns which can lead to these various evolutions.

With the previous analysis, some conclusions can be learnt from this set of experiments. First of all, among all mechanisms mentioned in section 2.3.3, the low-level convergence appears to be in this case the best element to explain the triggering of deep convection. In addition a convergence line enables convection to organize in a linear structure. But low-level winds features are also essential to sustain the linear organization. Indeed, it is when the flow is quite perpendicular to the squall line that convection is most efficient. As a result, the sensitivity to

the flow in the first kilometers of the troposphere is relevant. Thus, the location of the low-level pressure meso-low has a strong impact on the event modeling.

4.2.2 Physical study of the case with numerical models

4.2.2.1 Squall line environment

All experiments previously analysed allow a better understanding of atmospheric features which led to the severe squall line on 4^{th} October 2007. Next interpretations mainly lean on WRFcep simulation in which the squall line is rather well captured, and which enables to further explore the squall line environment only briefly described in section 2.3.1. First stage will be dedicated to the analysis of weather patterns at triggering time.

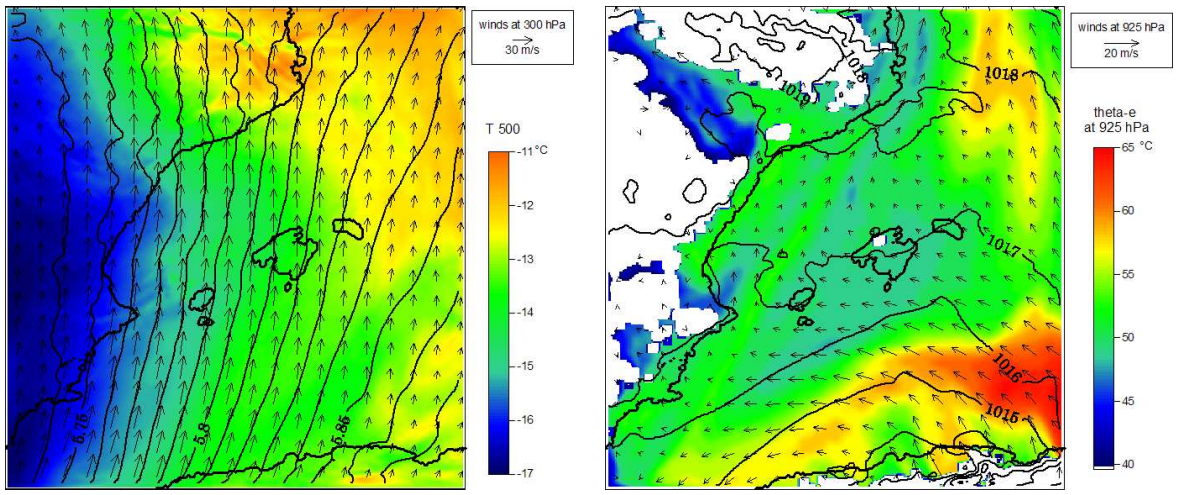

(a) (b)

Figure 4.5: Weather patterns at 6 UTC with WRFcep: (a) geopotential (kmgp) and temperature ($°C$) at 500 hPa and winds ($m.s^{-1}$) at 300 hPa, (b) EPT ($°C$) and winds ($m.s^{-1}$) at 925 hPa and mean sea level pressure (hPa).

At 6 UTC, even though low-level patterns show certain spread among experiments, the situation aloft tends to show clearly defined elements in a general agreement. Geopotential height and temperature at 500 hPa, displayed in figure 4.5-a, indicate a low centered over mainland Spain affecting also Alboran sea. In particular, the maritime area between Murcia region and Africa is affected by cold air in mid-troposphere. In the upper troposphere, a strong southerly jet streak goes along the eastern edge of this low. It can be infered from this figure that, aloft, features were favourable to convective developments all along the Spanish coast as far as to Tarragona. However, low-level patterns will define the likely place of the convective initiation. Figure 4.5-b presents the map of EPT at 925 hPa also at 6 UTC. The easterly flow going along African seashore provides warm and moist air at low-levels which reaches the Spanish coast about the south of Murcia. With this remark, the location of potential convection triggering is drasticaly restricted to a small area characterized by a strong CAPE (between 800 and 1000 $J.kg^{-1}$) and mainly a very weak CIN. The sea level pressure shown in figure 4.5-b indicates a low centered over northern Africa which has to be associated to the strong upper-level forcing. This low pressure area induces an easterly flow over the southern Mediterranean, and therefore it has an important influence on the winds convergence along the thermal boundary. This effect is

thought to be magnified by the presence of the Atlas range which can be supposed to contribute to low just downstream of the mountains.

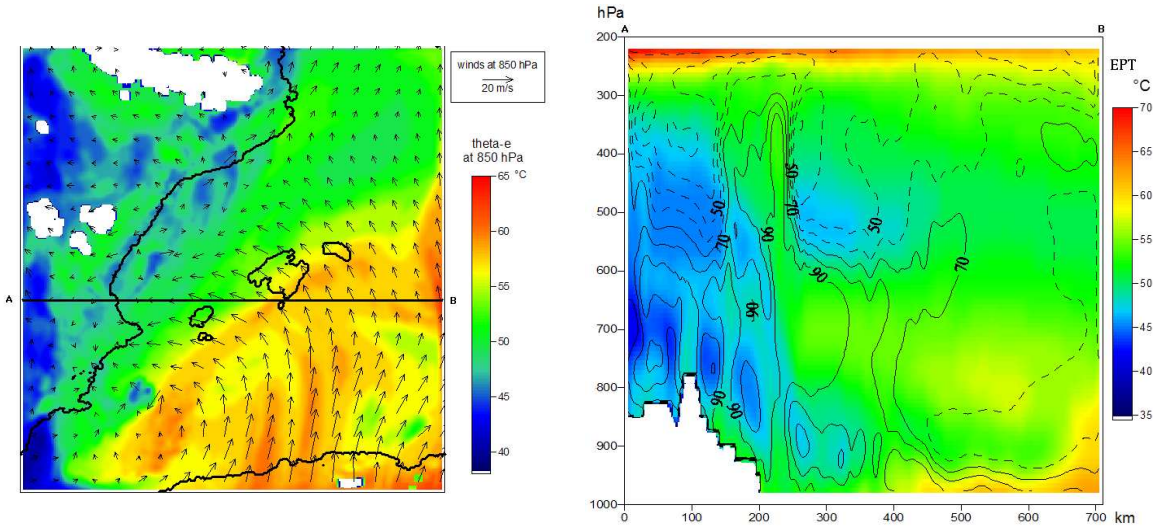

(a) (b)

Figure 4.6: Front features at 12 UTC in WRFcep experiment: (a) EPT and winds ($m.s^{-1}$) at 850 hPa, (b) vertical section A-B of EPT ($°C$) and relative humidity (continuous lines for values greater than 70 %, dashed lines otherwise).

After its triggering, the convective system evolves along the baroclinic boundary as shown at 12 UTC in figure 4.6-a which presents the equivalent potential temperature at 850 hPa. The location of the squall line can be easily identified thanks to the cold pool led at the rear. Stationary in its southern part, the northern part of this front moves westwards in the morning. Its vertical structure can be analysed with the figure 4.6-b that displays EPT and relative humidity. At low-levels, the front is characterized by a well-defined gradient of humidity and temperature presenting the classical structure of a cold front. However aloft, between 600 and 400 hPa, a dry and cold layer caps the front. Consequently this section looks like those obtained in katafronts, allowing convective developments in the warm area.

The baroclinic boundary is also characterized by a strong shear and especially near the Balearic archipelago as it is shown by figure 4.7. Due to the difference between the low-level easterly flow and strong southerly winds aloft, this sheared environment is favourable to sustain the once formed squall line. Shear values are on the whole greater than 20 $m.s^{-1}$ over the western Mediterranean and its direction is almost perpendicular to the squall line orientation. Such strong values allow to balance the vorticity created by thermal gradient near the gust front, and bring about efficient vertical updrafts. That is why the squall line life is quite long as this linear organization disappears around 20 UTC in WRFcep experiment, when it arrives in a less sheared area and after a signifiant weakening crossing the Mallorca orography.

4.2.2.2 Squall line internal features

To study the representation of the simulated MCS, we choose the MNHcep experiment which has the particularity to organize convection in a linear structure very close to radar observed

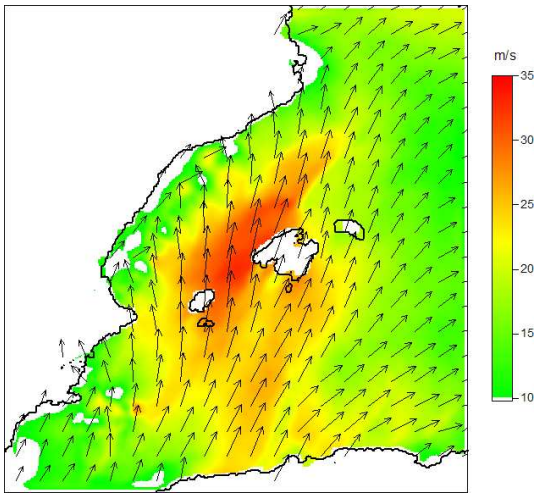

Figure 4.7: Horizontal wind shear between 700 and 1000 hPa greather than 10 $m.s^{-1}$ in WRFcep experiment at 11 UTC, with indication of shear direction.

reflectivities even though this simulation presents a temporal lag. The following analyses aim at showing that mesoscale numerical models are able to reproduce a squall line with features very close to the conceptual scheme presented in the first chapter.

On the sea level pressure chart plotted in figure 4.8-a, characteristics described in section 1.3.3 are well identifiable. Below the rainfall area, as a consequence of cooling by evaporation, a surface high is clearly marked with a pressure increase up to 5 hPa in some places in comparison to surrounding environment. Ahead the most active part of the squall line, a pre-squall meso-low is present. Indeed, vertical section of vertical velocity in figure 4.8-d indicates a subsident flow at mid-levels in front of the convective part, able to generate a low ahead of the convective part. In addition, under the stratiform part, the wake-low is also well sinulated, with a weaker magnitude than the pre-squall meso-low. Thus, pressure characteristics in this experiment are consistent with the squall line conceptual scheme and with observations registered at Santa Ponça station (figure 2.1).

Vertical sections easy the analysis of the simulated squall line. Reflectivites in figure 4.8-b point out a multicellular organization, proper to squall lines, with cells in different life cycle stages. The mature cell characterized by strong reflectivities in the whole troposphere is the place of severe updrafts reaching more than 20 $m.s^{-1}$ at mid-levels (figure 4.8-d). Another cell is forming ahead as it can be infered from high reflectivities until 4 km in front of the mature cell. At the rear, remains of old cells are identifiable, progressively incorporated in the stratiform part as in a multicellular thunderstorm.

Dynamics favouring the squall line sustainment can be understood with the EPT section displayed in figure 4.8-c. The descending rear inflow jet characterized by cold and dry air enhanced by rainfall evaporation is present under the stratiform part. Reaching the surface, this RIJ contributes to create the density current necessary to heighten updrafts in the convective part as a result of low-level convergence. Updrafts are located just ahead of the boundary between the cold pool and the moist environment, where the thermal gradient is high. As seen in the conceptual scheme presented in figure 1.1, horizontal vorticity generated by the bouyancy gradient is able to balance the opposed vorticity associated with the low-level shear.

Moreover, stratiform region dynamics physically interpretable with vertical velocities (figure 4.8-d) are in good agreement with the conceptual model exposed in figure 1.3. Just at the

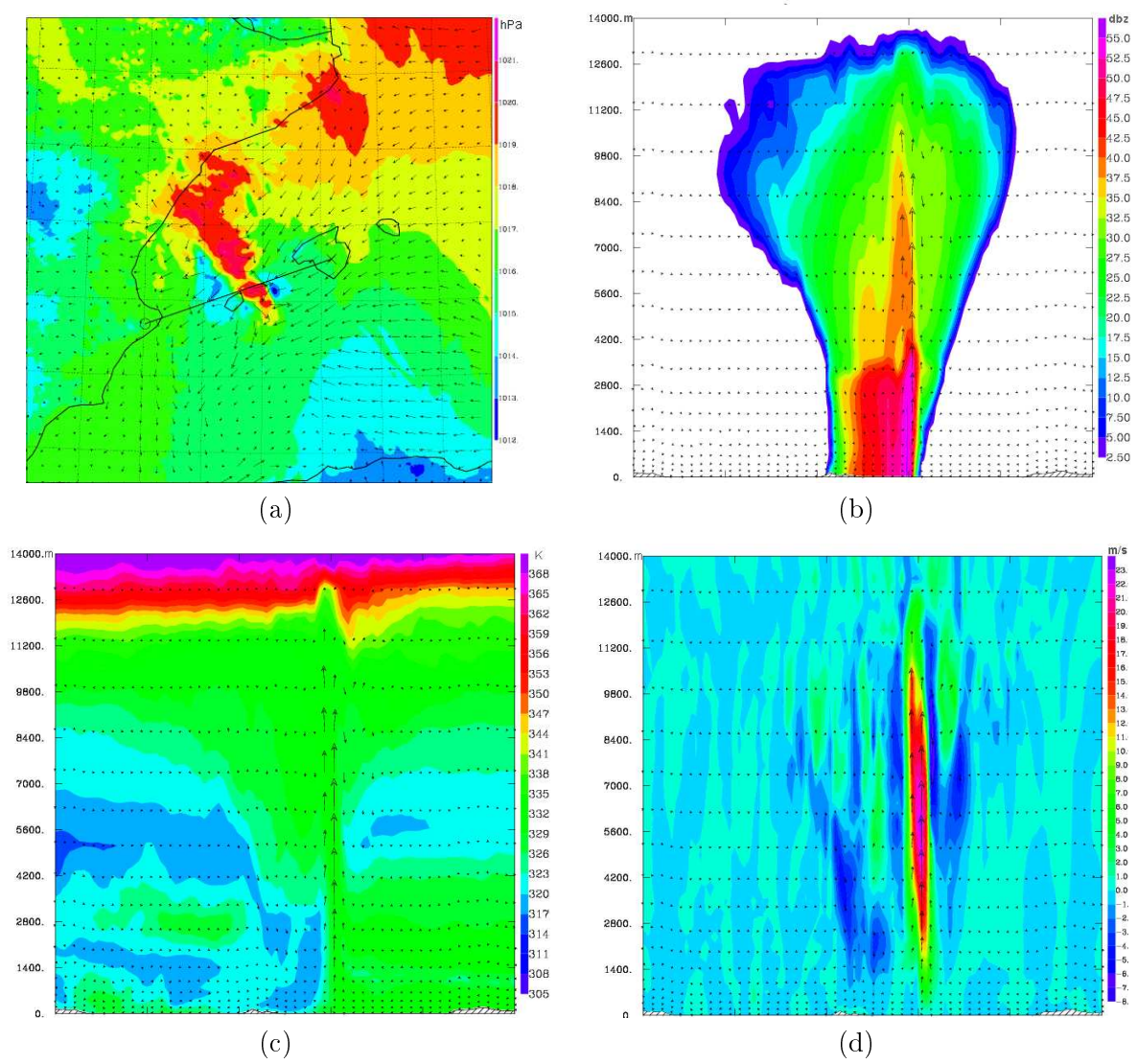

Figure 4.8: Squall line features in MNHcep experiment at 12 UTC; (a): Sea level pressure and surface winds, (b), (c) and (d): vertical sections of reflectivities, EPT, and vertical velocities respectively, with tangent winds, along the segment plotted on (a).

rear of the convective part, a transition zone of downdrafts is present whereas mesoscale updrafts only appear in a more distant zone of the stratiform part. In addition, downdrafts are associated with precipitation below the stratiform region. Eventually, all previous remarks tend to prove that the MCS simulated in this experiment presents all the dynamical features characterizing a squall line. These findings allow to investigate, with a higher resolution, signs of the presence of a favourable environment for tornadogenesis.

4.2.2.3 Tracking tornadoes

The goal of this part is to see whether a so well simulated squall line is able to produce mesovortices, essential tornado precursors. To track mesorvortices, which use to be characterized by a few kilometers size, the simulation MNHcep is not enough fine with its 2.4 km mesh. Therefore the idea is to run an experiment with a very high resolution, set to 600 meters, later called MNH_{600m}. Due to computational limits, this simulation has to be performed on a small

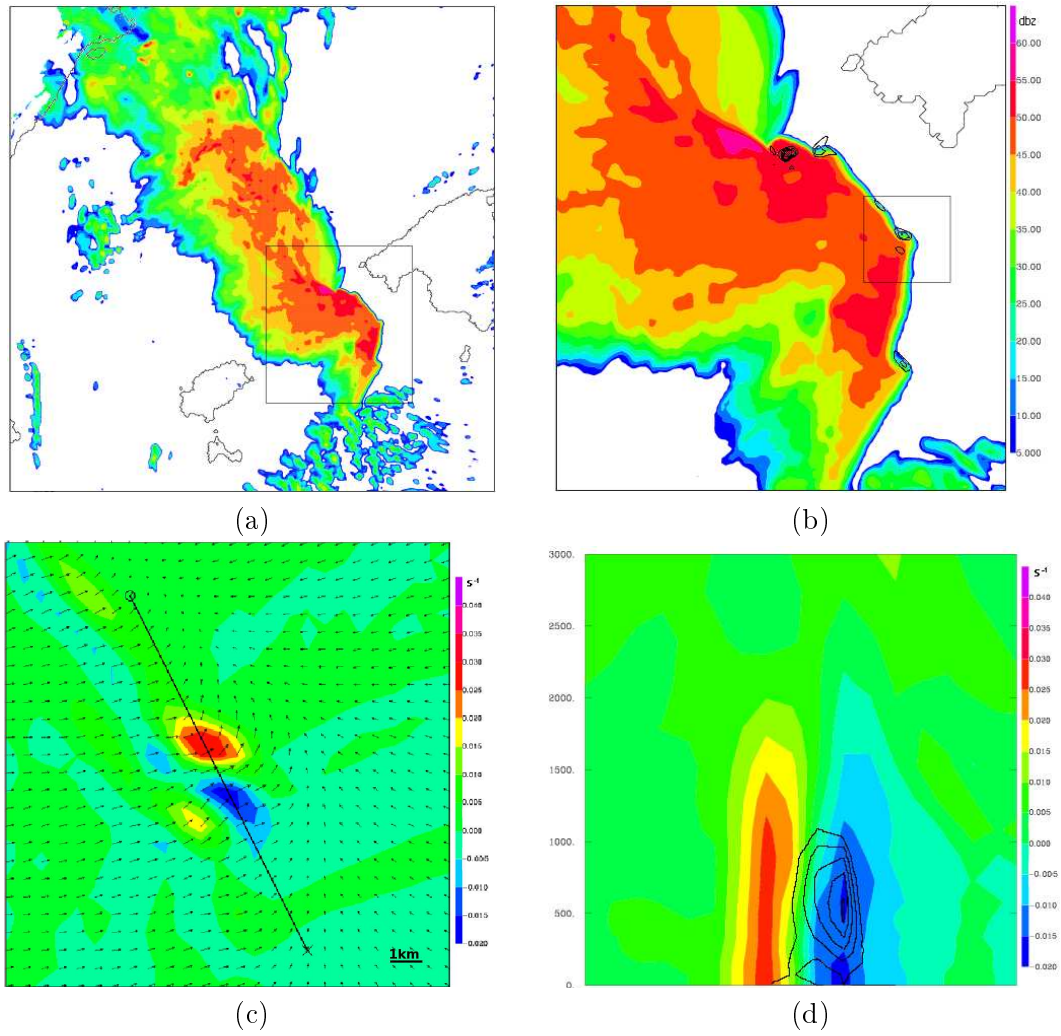

Figure 4.9: Very high resolution simulation MNH_{600m} at 12h30 UTC; (a): reflectivities at 200 m and indication of (b) domain, (b): zoom of (a) with positive vertical vorticity at 200 m (contoured in black from 1.10^{-2} s^{-1} to 6.10^{-2} s^{-1} every 1.10^{-2} s^{-1}) and indication of (c) domain, (c): vertical vorticity and horizontal wind at 200 m, (d) cross section according to (c) of vertical vorticity with negative values of vertical velocity contoured in black from 0 $m.s^{-1}$ to -5 $m.s^{-1}$ every 1 $m.s^{-1}$.

domain and during a short period. Consequently, it is initiated by MNHcep output, when the squall line is already formed at 12 UTC, on a small domain enclosed in D_1 including the whole squall line. Méso-NH is run during an hour and its boundary conditions are also provided by MNHcep. Physical parametrizations are the same than in MNHcep, thus the only difference is a four times higher resolution.

From the beginning of the simulation a bow echo is conspicuous in radar reflectivities in the southern part of the line. This convective organization was already present in initial conditions at 12 UTC, and it remains all the simulation long, curving progressively. In figure 4.9-a, which also presents the geographical domain of the simulation MNH_{600m}, it is clearly visible that the bow echo has some undulations on its leading edge and especially one develops just north of its apex. Near the bow center, a weak rainfall area must be linked to a strong RIJ bending the bow echo. Figure 4.9-b proves that each one of these undulations, generated by differences in outflow magnitudes, is the area of enhanced cyclonic convergence. Therefore, this high resolution

simulation allows to point out mesovortices, and particularly one is simulated on the cyclonic side of the bow apex.

Particular attention is paid to bow echo apex mesovortices which appear 15 minutes after MNH_{600m} beginning. As it is shown in figure 4.9-c at 12h30 UTC, a couplet of vortices with opposite circulations evolves near the bow apex, exactly where the RIJ is strongest. Their radius of about 1 km demonstrate the necessity of a high resolution mesh to capture such circulations. The fact that the cyclonic mesovortex is located to the north of the anticyclonic one indicates that the genesis of mesovortices couplet can not match with the classical conceptual scheme proposed by Trapp and Weisman (2003) and displayed in figure 1.6. This organization demonstrates that the transformation of horizontal vorticity born by baroclinic effect (see the EPT gradient in figure 4.8-c) into vertical vorticity is produced by updrafts. The cross section in figure 4.9-d shows that the area between the two vortices is characterized by downwards motion. The interaction of this downdraft with the surface may have produced a local updraft maximum just ahead of the gust front, necessary to tilt horizontal vortex lines. These results are a good illustation of the recent conceptual model of Atkins and St. Laurent (2009-b) presented in figure 1.7.

Life cycles of such simulated mesovortices are quite short. Positive and negative vortices magnitudes during the simulation MNH_{600m} are plotted in the graph 4.10. The two vortices develop at the same time and later the cyclonic vortex grows more to reach a magnitude three times greater than the anticyclonic one. Such evolution is thought to be caused by the Coriolis force influence as mentioned in section 1.3.5. Once arrived in Mallorca, mesovortices magnitudes significantly decrease. However, the sudden enhancement of cyclonic mesovortex occurs when the northern part of the bow echo collides with the Mallorca orography. A plausible hypothesis may be that such rubbing could slow down the bow echo north part and thus increases the cyclonic rotation just north of the appex. This theory can give a track to explain mesovortex formation over the bay of Palma during the event.

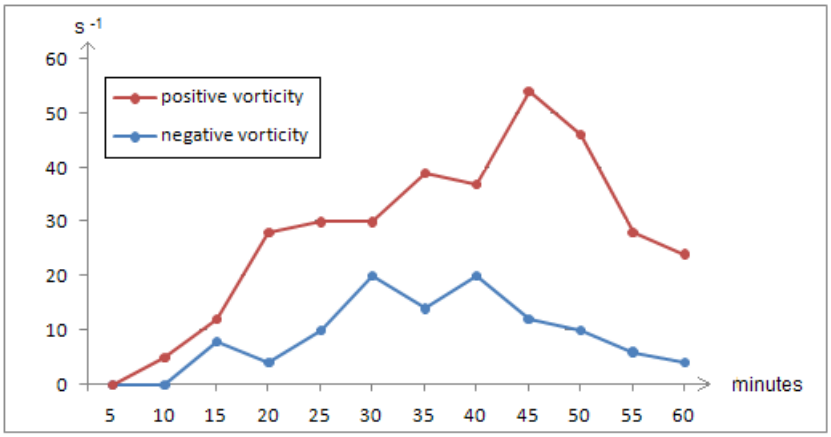

Figure 4.10: Bow echo apex mesovortices magnitudes at 200 m, cyclonic vortex in red, anticyclonic vortex in blue.

4.2.3 Initial conditions influence

With the ensemble of Méso-NH experiments, it is possible to discuss the importance of a good representation of initial conditions to lead to a correct modeling of the event. With the three available analyses, results are quite diverse and, particularly, simulations run with ALADIN are rather incorrect from the first hours. As expected, differences pointed out by figure 4.1 influence the triggering and the location of the convection. More precisely, the convergence line

present on ALADIN initial conditions explains the development of convective cells to the south of Balearic archipelago during the first hours of the simulation. As a result, simulations MNHala and MNHalaN failures are directly asribable to initial imprecise initial conditions. Consequently, no more investigations will be done with ALADIN analyses.

As concerns the comparison between ECMWF and ARPEGE initial conditions influence, the triggering of the cell which later becomes the squall line differs. In simulations with ARPEGE analyses, it is a clear response to a low-level convergence line along the thermal boundary, with a tendency to generate too many initial cells. However in ECMWF simulations, convergences are weaker and the triggering occurs to the west, in the favourable area previously mentioned. Another element in favour of ARPEGE analyses can be the fact that the precipitating system present along the thermal boundary over Balearic Islands in the morning is in a good agreement with radar observations (figure 2.3-a). On the contrary, simulations with ECMWF create a line of convective systems along the coast of mainland Spain as a consequence of the tongue of warmer air mentioned in section 4.1. Finally, a precise representation of weather patterns at initial time is very important to succeed in modeling this kind of Mediterranean events. Besides, another source of uncertainties in such simulations is due to boundary conditions, as it will be discussed in the next section.

4.2.4 Boundary conditions influence

Comparing nested experiments with those directly forced by analyses is a way to characterize the influence of boundary conditions. However, it must be remembered that this approach, in a case study configuration which uses analyses instead of forecasts, will not allow to fully investigate the grid nesting influence. In order to understand this later impact, it would be preferable to perform experiments substituting global analyses by forecasts of the same models.

Analysing differences between simulations MNHcep and MNHcepN allows to understand why only MNHcep succeeds in creating a cell separated from the coastal precipitation area. As shown by figure 4.2 (a) and (d), flows between those two simulations are not consistent especially in the triggering area. At 9 UTC, winds are significantly stronger in MNHcepN in the whole domain and do not converge offshore of Murcia as in MNHcep. On the contrary the southwest part of the domain is affected by weak winds. As these two experiments only differ in their boundary conditions, a study of meteorological parameters out of domain D_1 limits may explain such differences. In particular, some contradictions can be underlined on the geopotential height at 850 hPa plotted at 12 UTC between ECMWF analysis (fig 4.11-a), which are MNHcep boundary conditions, and parent model grid in MNHcepN experiment (fig 4.11-b). The analysis of these figures confirms an observation already apparent six hours earlier. A low pressure area affecting southeastern Spain is weaker in ECMWF analysis than in charts computed by Méso-NH. Furthermore, the geopotential gradient is higher over the Mediterranean sea in MNHcepN boundary conditions. These low-level environments will be transmited into each simulation respectively, and as a result, in MNHcepN simulation the pressure chart at triggering time near the boundary layer top is significantly different from the chart of the MNHcep experiment. Stronger winds computed in this case are consequently a response to the higher gradient in boundary conditions. Shape and position of the low at 850 hPa prevent the triggering of a cell offshore of Murcia in MNHcepN simulation, an area characterized by a disorganized low-level flow.

The comparison between WRFcep and WRFcepN leads to the same conclusions: the presence of stronger winds over the sea and a higher gradient of geopotential at 850 hPa. However this time the triggering takes place but too late. Differences between MNHarp and MNHarpN are less obvious, even if boundary conditions computed by Méso-NH also present a tendency to

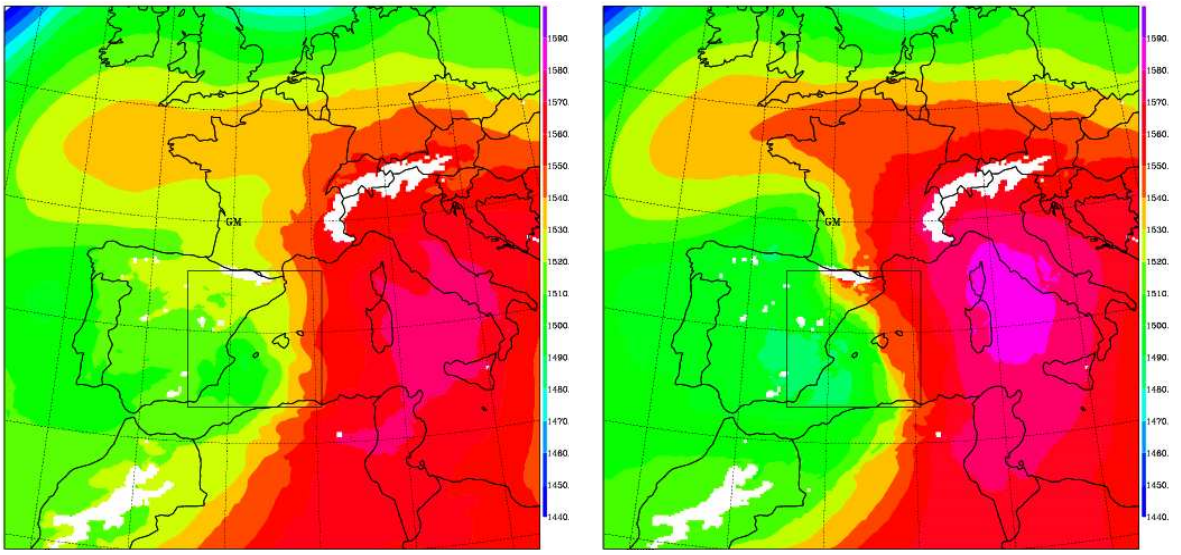

(a) MNHcep (b) MNHcepN

Figure 4.11: Boundary conditions of the high resolution simulation: geopotential (mgp) at 850 hPa at 12 UTC for CEP analysis (a) and MNHcepN parent forecast (b).

increase the low-level pressure gradient. But here, with ARPEGE analyses, the convective initiation seems tied to a more marked convergence line along the front, feature more ascribable to initial conditions. However, light differences in wind chart at triggering time bring about higher differences in cells development along the convergence line. In MNHarp experiment, two near and independant cells evolve separately (B1 and B2) whereas they are more distant in MNHcepN (E0 and E1). This allows the second cell E1 to be out of the first one outflow influence. This constatation is a good illustration that the squall line modeling is highly sensitive to the initial environment.

We can wonder what is the cause of such differences between these boundary conditions. Logically, a simulation using grid nesting would present a better transition between large scale analyses and the fine resolution simulation. However, analyses have the huge advantage to be the result of a process of data assimilation, which improves the atmosphere representation. On the contrary, during the simulation with grid nesting, observations available in the parent domain are not used, and this damages those experiments. For example, geopotential height at 850 hPa measured by soundings at 12 UTC are summarized in table4.1, where they are compared with data of MNHcep and MNHcepN experiment. Observed data are closer to MNHcep surrounding conditions, and even if values are slightly weaker, the gradient of pressure is nearly the same. On the opposite, in MNHcepN this zonal gradient is too strong, as shown in particular by Nîmes and Santander observations. The basic role played by observations over the Mediterranean regions is again demonstrated.

4.2.5 Model influence

Simulations run with Méso-NH, WRF and MM5 models on the domain D_1 directly forced by ECMWF analyses enable to compare each model performance to capture the squall line. A first analysis will concern the squall line triggering. In the three experiments, a convective cell develops near the southwest corner of the domain at 8 UTC but then follows different kinds of evolution. In WRFcep simulation, it continues to grow and steadily acquires a squall line structure, whereas in both other simulations, it dies before 10 UTC. In the MNHcep experiment,

City	sounding	MNHcep	MNHcepN
Nimes	1554	1546	1562
Santander	1536	1520	1481
Palma	1527	1526	1525
Madrid	1531	1519	1492
Murcia	1539	1506	1488
Alger	1550	1530	1510

Table 4.1: Geopotential height at 850 hPa (mgp) measured by several soundings at 12 UTC, compared with data in MNHcep and MNHcepN experiments at the same time.

another cell further developed to the north, prevents the easterly flow to reach this cell. In the case of MM5cep, the model seems not to be able to sustain the initial cell, whereas the environmental features are very close to those of both other experiments. Although differences at about 8 UTC are minor, they magnify later to lead to very different evolutions.

A blatant difference which appears in figure 4.2 for MM5 simulation is the absence of convection along the coast at 9 UTC whereas it begins before 8 UTC in both other simulations. This area corresponds to the boundary between an easterly low-level flow to the south, due to a low over Africa, and a southerly flow affecting regions out of this influence, more at the north and aloft. A plausible hypothesis is to attribute such differences to model physical schemes and more precisely to PBL scheme used in MM5, which seems less efficient to trigger convection. This hypothesis will be tested in section 4.4.1.

As it can be infered from figures 4.2, 4.3 and 4.4, which present different realization of three evolving scenarios, a multi-model strategy is very useful to predict this kind of deep convection, evolving over the sea and where convection triggering can not be attributed to coastal orography. Each model has its own physical and dynamical particularities and resorting to several models is an interesting way to cope with the forecasting uncertainties at this high resolution. Moreover, previous sections have shown that if a multi-model approach can be combined with several initial conditions, simulations sample increase and the more varied the simulations are, the higher is the likelihood to encompass plausible solutions within the ensemble of forecasts.

4.2.6 Conclusions of the comparative study

The comparative analysis of particularities of each simulation has led to the following conclusions. First of all, the quality of an experiment is mainly dependent on its ability to trigger a cell offshore of Murcia early in the morning. Such triggering is closely tied with an area of low-level winds convergence and its absence conducts to simulation failures. The best simulations show a very realistic representation of the squall line, including mesovortices ahead of the gust front, that confirm the presence of a favourable environment for the genesis of small vortices, including tornadoes. They have also allowed a better understanding of weather patterns able to generate such devastating squall line, showing particularly the importance of the convective instability associated with a katafront, and the relevant influence of low-level shear to sustain the linear organization.

Study of initial conditions from several analyses has demonstrated their importance in convective initiation through the location of a convergence line. In addition, simulations tend to produce better results with a direct forcing by coarser analyses. This observation shows the essential role played on this case by data assimilation to improve boundary conditions quality. Differences pointed out in experiments performed with the three mesoscale numerical models

indicate the benefits of a multi-model strategy, as each one is characterized by its own physical and dynamical parameterizations. Next sections are devoted to present results of attempts to improve the convective triggering of MM5cep experiment with two different approaches. The first one resorts to pseudo-observations assimilation and the second points out the role played by PBL parameterizations in the convective initiation. Finally, the Atlas range influence on the triggering location of the squall line is studied.

4.3 Initialization of convection with subjective data assimilation

4.3.1 Description of the method used

Since the experiment MM5cep presents a bad initiation without low-level convergence in the morning, the idea is to create artificially a convergence line to check whether it can allow the triggering of deep convection and improve the further evolution. As shown in the previous section, the lack of observations over the sea can be the cause of a bad capture of weather patterns leading to a convergence line. A solution can be to generate pseudo-observations using a simulation which succeeds in triggering a cell with a convergence line in good spatiotemporal agreement with satellite and radar data. Since MNHarp experiment reproduces the best modeling of the triggering with a stationary stage, it will be interesting to add pseudo-observations in order to try to reconstitute a low-level environment similar to MNHarp.

To reproduce such mesoscale structure, it is planned to assimilate several wind observations affecting the low-levels, with a small radius of influence set to 30 km. In order to take the temporal dimension into account, each observation will be nudged over a time window of 40 minutes before and after the observation. On the vertical, observations will be added in levels spaced by 0.04 sigma units in the PBL (approximatively 40 hPa) with a vertical radius of influence corresponding to 0.025 sigma units. The wind nudging coefficient $G_{\overrightarrow{v}}$ is set to 10^{-2}, a very high value which allows to really drive the model solution towards observations. Among variables which can be assimilated, only wind data will be provided as pseudo-observations in this exercise.

The experiment with nudging (MM5nud) is performed with ECMWF analyses using the same parameterizations than in MM5cep. In addition, pseudo-observations are supplied at 8 and 9 UTC, therefore assimilated between 7h20 and 9h40 UTC, in order to create the convection triggering which is absent in MM5cep. Wind data provided to the model are inspired from MNHarp simulation results at 8 and 9 UTC in the PBL, where differences are important between simulations. Pseudo-observations provided at 8 UTC are summarized in figure 4.12. Blue arrows correspond to observations assimilated at three sigma levels, approximately between the surface and 900 hPa, to reproduce an homogeneous profile in such layer. Red arrows are data supplied at 866 hPa, in agreement with MNHarp winds chart near the PBL top. Pseudo-observations are only added in the southwestern part of D_1, since elsewhere wind directions and speeds are close in MM5cep and MNHarp. As illustrates figure 4.12, the low pressure area location is aimed to be corrected thanks to such pseudo-observations, that allow to introduce a new circulation which generates a well defined convergence line in the whole PBL at 8 UTC. In order to try to initiate the stage of slow eastwards moving of the convection, pseudo-observations provided at 9 UTC are exactly the same, but displaced 30 km eastwards.

4.3.2 Results

Reflectivities and low-level winds are plotted for MM5nud simulation in figure 4.13 at 9 UTC (a) and 15 UTC (b). These charts have to be compared with those of MM5cep simulation (figures 4.2-i and 4.4-i). At 9 UTC an already well developed cell is present just over the area where the convergence is the strongest. The stationarity stage is correctly reproduced from 8

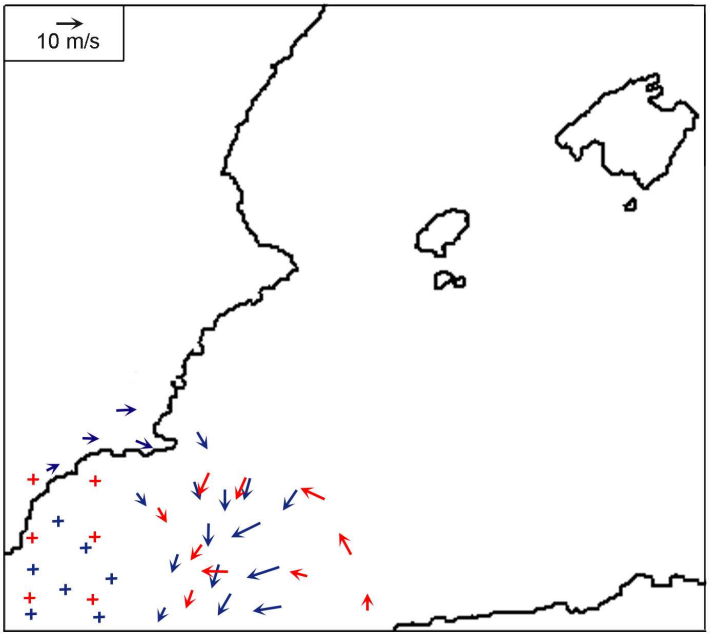

Figure 4.12: Pseudo-observations assimilated at 8 UTC in MM5nud experiment, blue arrows are data provided at sigma levels corresponding to 982, 942 and 906 hPa, red arrows at 866 hPa.

to 9 UTC with a light eastwards moving, which remains however less important than in remote sensing observations. Winds features are nearly the same as in MNHarp simulation at triggering time, thanks to the high value set to the nudging coefficient. Thus, the objective to force the convection triggering in the accurate place is accomplished. Afterwards, the correct evolution of this cell and its progressive transformation into a squall line prove the importance of a good initiation. On figure 4.13-b, the situation obtained at 15 UTC is very close to observations, with a clear squall line which reaches Mallorca around this time. Although it remains slightly to the north, reflectivities chart at 15 UTC is very similar to those observed by the Spanish radar network (figure 2.3-d). This slight spatial lag can be interpreted as a consequence of the failure to correctly capture the initial eastwards movement associated with the V-shaped thunderstorm. Nevertheless, results obtained in this simulation are very satisfactory.

The comparison between MM5cep and MM5nud experiments leads to interesting conclusions even though some questions remain. First, it clearly shows that the convective initiation is basic to later succeed in reproducing the squall line with correct spatiotemporal features. Therefore, scarce observations over the sea are crucial for numerical models to capture mesoscale features such as convergence lines. However in this case, many observations are assimilated at several levels. From an operational point of view, we can wonder whether a few additional surface data assimilated in coarse resolution analyses could be enough to significantly improve mesoscale forecasts. Although it was shown in the previous section that it is possible to obtain a correct simulation with good initial an boundary conditions, it could be interesting, in addition, to resort to an assimilation technique such as observational nudging to complete the commonly used cycle of assimilation which improves the analyses. Indeed, if we consider a forecast beginning at t_0, a time windows until t_1 is used to produce t_0 analysis. Thus, all the observations available between t_0 and t_1 could be assimilated by observational nudging.

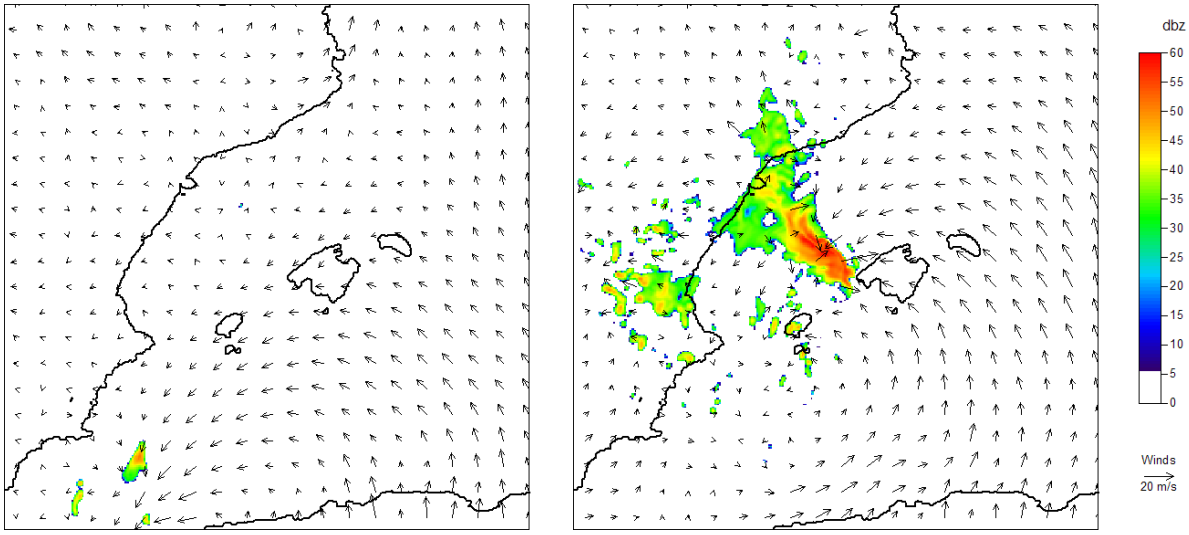

(a) 9 UTC (b) 15 UTC

Figure 4.13: Reflectivities at 800 hPa and winds at 925 hPa for MM5nud experiment at (a) 9 UTC, (b) 15 UTC.

4.4 Sensitivity experiments

4.4.1 Influence of planetary boundary layer scheme

Reflectivities and low-level winds simulated in the experiment MM5pbl carried out with ETA scheme are displayed in figure 4.14, after the convective triggering and at the mature stage. These charts are clearly different from those obtained with MRF scheme presented in figures 4.2-i and 4.4-i. Unlike the uncorrect evolution of the reference simulation MM5cep, this simulation with the new PBL scheme is significantly better. The convective initiation takes place at 7 UTC offshore of Murcia, but slightly too south. Other convective cells are also present along the Spanish eastern coast. Consequently, the ETA scheme appears to be more favourable to trigger convection in this case. After a rather correct initiation, the model creates a squall line presenting a good evolution despite a light delay which seems to be the consequence of the convective triggering spatial lag. Next paragraph will focus on the differences in the PBL structure between the two simulations, in order to understand why MRF scheme does not enable early convective initiation.

The comparison of vertical profiles averaged over the maritime triggering area D_5, displayed in figure 4.14, shows light differences in the PBL, but sufficient to lead to distinct convective initiations. The moisture with ETA scheme is higher in the layer below 950 hPa, whereas in the upper PBL the environment is drier than with MRF scheme (figures 4.15 and 4.16). In the lower PBL the MRF profile is more mixed, presenting a mixing ratio of water vapor approximately constant. On the contrary, with ETA scheme, this ratio is higher nearby the surface and linearly decreases with height. Other comparative elements are indicated in table 4.2. The potential temperature gradient between 1000 and 950 hPa confirms the well-mixed layer in MRF case. The moister layer above the surface with ETA decreases the free convection level and consequently the CAPE for a surface parcel is higher in the profile 4.15-b. In addition, the CIN in the domain D_5 remains very weak. Winds simulated with ETA scheme near the surface are slightly stronger and present a more northerly direction. These two elements are favourable to generate an enhanced convergence in the triggering area. Moreover, stronger winds allow higher evaporation from the sea, as shown by the difference of latent heat flux between the two PBL schemes. This

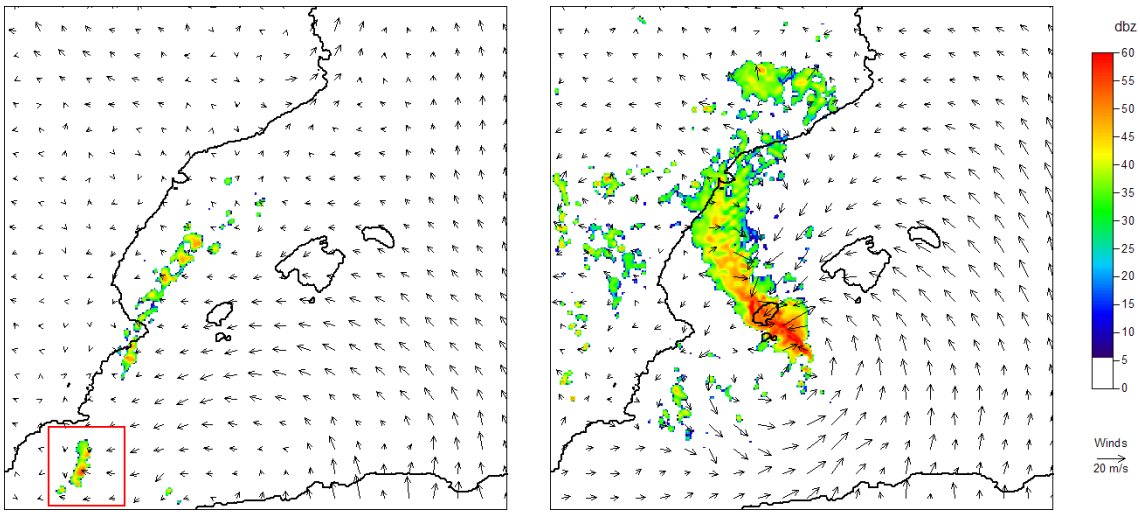

(a) 9 UTC (b) 15 UTC

Figure 4.14: Reflectivities at 800 hPa and winds at 925 hPa for MM5pbl experiment; (a) at 9 UTC and domain D_5 later used, (b) at 15 UTC.

evaporation can contribute to the colder and moister environment in the convective boundary layer.

Finally, this sensitivity experiment proves the relevant influence of the PBL scheme on the deep convection initiation, whose pameterizations are essential to well simulate severe weather maritime events. In the case of 4^{th} October 2007, ETA scheme leads to a better modeling of the squall line thanks to a rather correct convective initiation, absent in the simulation with MRF scheme. The local approach used in ETA scheme associated with an 1.5 order prognostic TKE closure, as in Méso-NH and WRF PBL schemes, is favourable in this squall line case to trigger convection. On the opposite, a scheme as MRF, using an 1 order closure and K-profiles to represent eddy coefficients leads to a well mixed convective boundary layer which decreases the convective instability. The earlier convective development with ETA scheme can be attributed to the slower diffusion of mesoscale energy to subgrid turbulent structures. This allows to retain an amount of energy to initiate convection. On the contrary, MRF scheme provides too much energy to its turbulent scheme, were it is dissipated by viscosity. It will be interesting to complete this sensitivity experiment with other cases of maritime deep convection to see whether this tend is confirmed.

PBL scheme	MRF	ETA
Potential temperature at 1000 hPa ($°C$)	20.6	20.3
Potential temperature at 950 hPa ($°C$)	21	21.2
CAPE ($J.kg^{-1}$)	1138	1344
CIN ($J.kg^{-1}$)	4	6
wind direction at 1000 hPa ($°$)	66	59
wind speed at 1000 hPa ($km.h^{-1}$)	12.9	13.4
Latent heat flux ($W.m^{-2}$)	66.8	75.1

Table 4.2: Comparison of some parameters averaged in the triggering area D_5 at 6 UTC for MRF and ETA scheme.

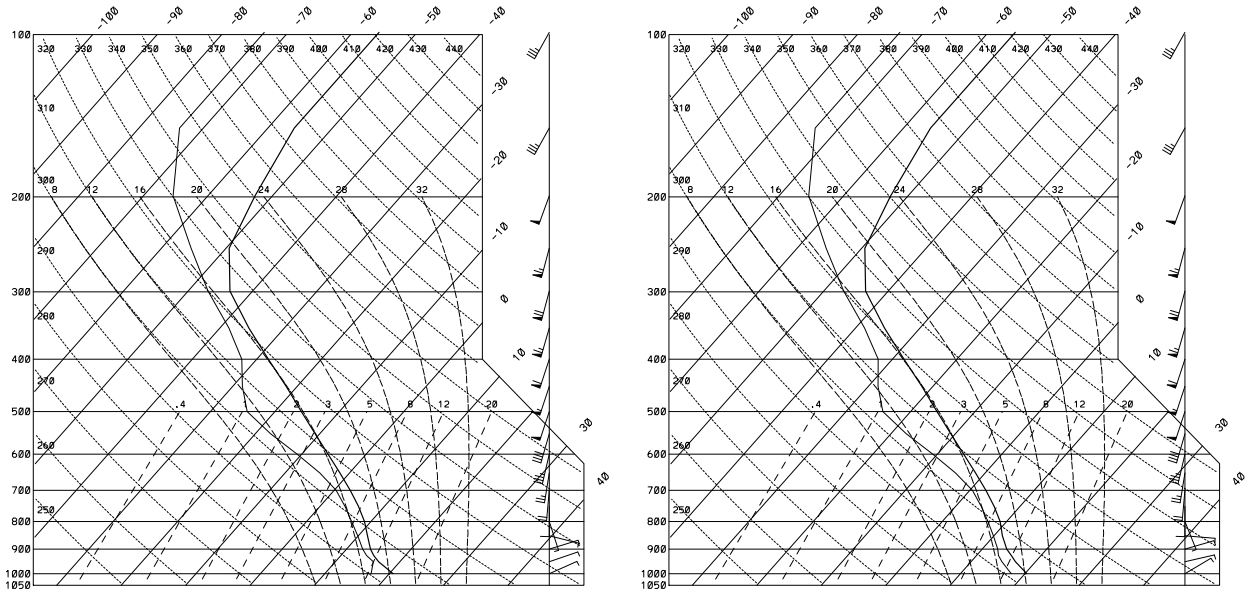

(a) MRF (b) ETA

Figure 4.15: Comparison of vertical profiles for simulation with MRF and ETA PBL schemes at 6 UTC in the triggering area D_5: (a) Vertical profile of MM5cep simulation averaged on D_5, (b) idem for MM5pbl.

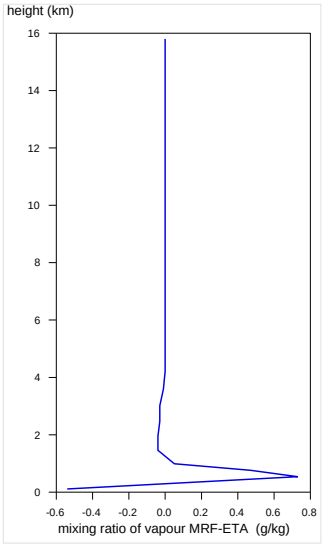

MRF-ETA

Figure 4.16: Difference of mixing ratio of water vapor between figure 4.15 profiles.

4.4.2 Atlas influence

The simulation WRFatlas without African orography succeeds in initiating a convective cell near the location of squall line triggering in WRFcepN, but slightly to the west (figure 4.17). In addition, the coastal convection also presents a similar evolution. In both experiments, there is a line of convergence along the thermal front, but low-level winds in the south of the domain are logically stronger in WRFatlas experiment due to the absence of mountain drag.

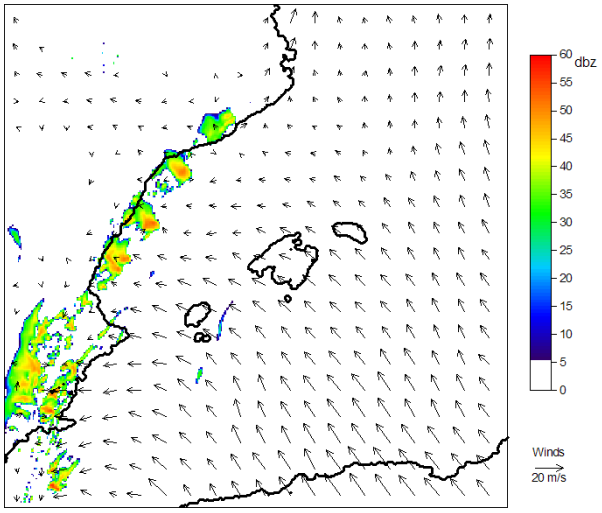

Figure 4.17: Reflectivities and winds at 925 hPa for WRFatlas experiment at 9 UTC.

Atlas influence is brought to light by figure 4.18. The difference between wind charts of the two simulations represents the role exerted by the African orography. In the southeastern part of the domain, it reduces wind speed and does not change significantly the flow direction. However, D_1 southwestern part is more influenced by the orography which constitutes an important obstacle to the souteasterly low-level flow. In the simulation WRFcepN, a relative low pressure area (-15 *mgp* approximately) present downstream of the mountains over the southern Mediterranean Sea, is the consequence of the Atlas mountains. It affects wind distribution in the triggering area. Indeed, the low-level flow in the figure 4.2-h corresponding to the reference simulation WRFcepN has a more established easterly direction than in the simulation without African orography. Figure 4.18 clearly shows that the Atlas range alters the circulation, adding wind convergence offshore of Murcia. Such effect tends to misplace the convective triggering to the east.

Finally the presence of the Atlas mountain range is not a decisive factor to explain the convective triggering. The general easterly flow is the consequence of the dynamic low pressure area over Africa associated to the upper-level forcing. However, the effect of Atlas mountains is characterized by a zonal deviation of the low-level flow and an increase of the convergence which slightly improves the convective triggering location. Even though in this case, differences are not large comparing squall lines evolutions, it can be assumed that in simulations performed with Méso-NH forced by ARPEGE analyses, in which the low-level convergence is stronger and plays a more relevant role in the convective initiation, the circulation induced by the Atlas range has a prevailing effect on the convection triggering.

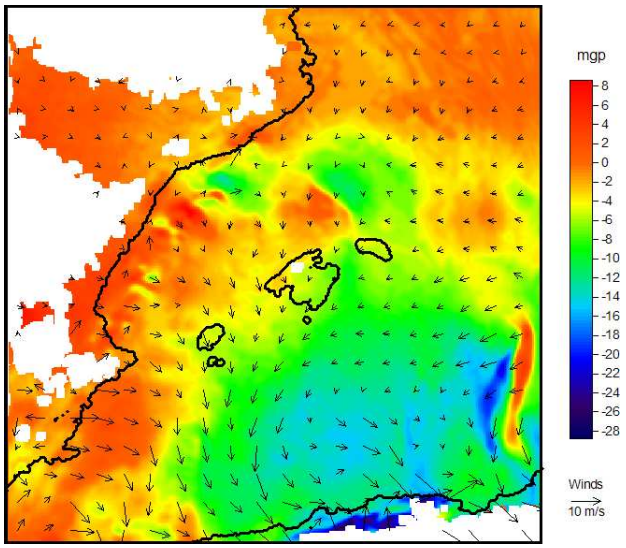

Figure 4.18: Influence of Atlas mountains on wind and geopotentiel height at 925 hPa, difference WRFcepN minus WRFatlas at 8 UTC.

4.5 Conclusions of complementary investigations

The first objective of these further investigations was to attempt an improvement of MM5cep which does not succeed in correctly initiating the squall line. In order to remedy this failure, two different approaches have been considered. The assimilation of pseudo-observations succeeds in creating a convergence line offshore of Murcia, which is enough to trigger the squall line in a good agreement with remote sensing data. The substitution of the PBL scheme indicates that an 1.5 order prognostic TKE closure scheme seems more adapted to initiate convection in maritime convective events. In summary, a dynamic and a thermodynamic way to trigger the convection have been achieved. Another objective was to understand Atlas mountain range influence on the circulation over the southern Mediterranean Sea. Although the circulation induced by the low pressure area downstream of the orography is not decisive to trigger the convection, it affects the convective initiation location.

Conclusions and outlooks

The aims of this study was to analyse the severe convective event of 4^{th} October 2007 that affected and strongly damaged the island of Mallorca. An observational study provided clues to consider the responsible mesoscale convective system as a short squall line with a maritime initiation early in the morning offshore of Murcia. The synoptic situation was characterized aloft by a cut-off over mainland Spain associated with cold air coupled with a jet streak and a pronounced positive potential vorticity anomaly. Its effect reached the surface, creating a low pressure area over North Africa inducing an esterly flow over the southern Mediterranean Sea. This area was also affected by a baroclinic boundary separating a moist and warm air mass over the sea from a drier and colder environment over mainland Spain.

An ensemble of numerical simulations performed at high resolution through a combination of three mesoscale models with different initial and boundary conditions has shown the crucial role exerted by a low-level convergence line to trigger and locate the convection. Its position is governed by an orographically-induced low pressure area over the southern Mediterranean basin. In addition, the low-level esterly flow is necessary to guarantee the squall line organization as it is proved by an unsuccessful simulation in which a previous outflow boundary perturbs the general flow. Best experiments indicate that the squall line evolves along the baroclinic boundary whose structure matches with a katafront. The cold and dry layer above its surface boundary enhances the precipitation evaporation rate, which strenghtens the squall line rear inflow jet. Moreover, the strong sheared environment appears to be decisive to sustain the squall line.

In this favourable environment, mesoscale models have shown their ability to reproduce a squall line convective organization, even though its spatiotemporal evolution is not always well captured. Particularly, the multicellular structure associated with the well-identified internal dynamics of a squall line is correctly simulated. A realistic experiment containing a bow-echo in the southern part of the squall line allowed to initiate a very high resolution simulation with a grid size of 600 meters centered on the convective system. This experiment indicates that a couplet of mesovortices develop in each undulation of the squall line gust front. Contrary to the widepsread conceptual model in which a downdraft tilts the tubes of horizontal vorticity baroclinically generated, in this case, mesovortices couplet genesis is due to updrafts.

Simulations which succeed in triggering a convective cell in correct conditions later develop a squall line. This analysis demonstrates the importance of a good convective initiation, closely related to a precise capture of the environment in the initial conditions. In particular, ALADIN analysis presents inaccurate initial flow features, that leads to simulation failures. Such differences in initial conditions over the sea are attributed to the lack of observations over the Mediterranean basin. In addition, experiments tend to produce better results with a direct forcing by coarse analyses than with grid nesting method. This conclusion demonstrates the crucial role played by data assimilation of the few observations available near the Mediterranean Sea, in order to improve global model analyses, used here as boundary conditions. Moreover, a

multi-model approach has shown its interest to cope with the forecasting uncertainties at high resolution. When it is combined with several initial conditions, it increases the likelihood to emcompass the plausible solution among the ensemble of forecasts.

Two different methods have been planned to remedy the failure of a simulation with MM5 forced by ECMWF analyses. The introduction of a synthetically generated convergence line by means of nudging data assimilation of wind pseudo-observations led to an accurate triggering offshore of Murcia and to a correct evolution of the squall line. This result proves the importance of the convergence line to initiate the convection in the 4^{th} October 2007 event. It also demonstrates, once again, the necessity of meteorological observations over the Mediterranean basin. Our case study illustrates that observational nudging method can be combined with the commonly used cycle of assimilation to improve not only initial conditions, but also model solution during the first steps of a forecast.

The second approach was to substitute the PBL scheme used in the daily "operational" runs at the UIB by a scheme using an 1.5 order closure and TKE equation. It allowed to initiate the convection earlier and consequently, it led to a better squall line modeling. This new scheme creates more convective instability due to a different vertical distribution of water vapor in the convective boundary layer. A scheme as MRF, producing a well-mixed layer, is less favourable to trigger convection in this maritime event. A too rapid diffusion of available mesoscale energy to the subgrid-scale turbulent eddies seems responsible for the delay of MRF scheme to initiate convection.

Finally, the role of Atlas range of mountains on the convective initiation has been analysed. Even though the flow perturbation downstream of this African orography is not a decisive factor to initiate convection, it increases wind convergence offshore of Murcia and thus slightly improves the triggering location. However, it is assumed that in events where the dynamic low-level southeasterly flow is not so pronounced, the Atlas influence can be essential to generate the convergence line and to trigger maritime convection.

To conclude, the success of a numerical simulation to capture a severe convective event with a maritime initiation closely depends on a conjunction of factors from distinct scales. On the 4^{th} October 2007 event, in a favourable synoptic environment which has been identified, a mesoscale circulation was necessary to lead to a precise triggering of the squall line. Lastly, the ability of mesoscale numerical models to reproduce such maritime convective event is highly dependant on initial condition accuracy.

Outlooks

This numerical study points to several interesting outlooks. First of all, the ability shown by mesoscale models to reproduce convective structures as squall lines fosters the idea of using an operational limited area model over the western Mediterranean basin. This would be profitable for all surrounding countries. The diversity of results obtained through the three mesoscale models also tends to encourage an ensemble forecasting strategy based on several models or various initial conditions. A probabilistic approach could be considered to complete individual model solutions. This strategy will help forecasters in their daily work. However, as demonstrated by this study, a sine qua non condition for accurate mesoscale forecasts in this area will require to mitigate the lack of observations over the sea. The development of a maritime observational network over the Mediterranean basin with buoys and equiped boats is thought to significantly improve severe weather forecasts in this area through a better quality of initial conditions.

After completion of previous investigations, other complementary studies can be planned. First, to complete this case study, it would be interesting to simulate the case with a forecast approach, i.e. without resorting to analysis to provide boundary conditions. Furthermore, it would enable a better understanding of nesting influence on simulations. Another point that is worth considering is the impact of Mallorca orography on mesovortices growth and location. More general studies can also be envisaged. First, a feasibility study could be carried out to assess the interest to adapt observational nudging of real or synthetical data to operational forecasts. Next, a systematic comparison performed on several convective cases, both maritime and continental, could lead to the conclusion to substitute MRF PBL scheme by ETA in the UIB daily "operational" forecasts. Finally, as concerns mesovortices, future investigations that focus on collecting high resolution observations with mobile Doppler radars should provide interesting elements to better understand which dynamical mechanisms prevail in mesovortices genesis.

Bibliography

[1] Atkins, N., and St. Laurent, N. Bow echo mesovorticies, Part I: Processes that influence their damaging potential. *Monthly Weather Review 137* (2009), 1497–1513.

[2] Atkins, N., and St. Laurent, N. Bow echo mesovorticies, Part II: Their genesis. *Monthly Weather Review 137* (2009), 1514–1532.

[3] Bougeault, P., and Lacarrère, P. Parametrization of orography-induced turbulence in a meso-beta-scale model. *Monthly Weather Review 117* (1989), 1870–1888.

[4] Browning, K. Conceptual models of precipitation systems. *Weather and Forecasting 6* (1986), 23–41.

[5] Caniaux, G., Redelsperger, J., and Lafore, J. A numerical study of the stratiform region of a fast-moving squall line. *Journal of Atmospheric Sciences 51* (1994), 2046–2074.

[6] Carlson, T., and Boland, F. Analysis of urban-rural canopy using a surface heat flux/temperature model. *Journal of Applied Meteorology 17* (1978), 998–1013.

[7] Clark, T., and Farley, R. Severe downslope windstorm calculations in two and three spatial dimensions using anelastic interactive grid nesting: A possible mechanism for gustiness. *Journal of Atmospheric Sciences 41* (1984), 329–350.

[8] Colella, P., and Woodward, P. The piecewise parabolic method (PPM) for gas dynamical simulations. *Journal of Computational Physic 54* (1984), 174–201.

[9] Cuxart, J., Bougeault, P., and Redelsperger, J. A turbulence scheme allowing for mesoscale and large eddy-simulation. *Quarterly Journal of the Royal Meteorological Society 126* (2000), 1–30.

[10] Ducrocq, V., Nuissier, O., Ricard, D., Lebeaupin, C., and Thouvenin, T. A numerical study of three catastrophic precipitating events over Southern France. Part II: Mesoscale triggering and stationaity factors. *Quarterly Journal of the Royal Meteorological Society 134* (2008), 131–145.

[11] Ducrocq, V., Ricard, D., Lafore, J., and Orain, F. Storm-scale numerical rainfall prediction for five precipitating events over France: on the importance of the initial humidity field. *Weather and Forcasting 17* (2002), 1236–1256.

[12] Fujita, T. *The Downburst, microburst and macroburst.* University of Chicago, Illinois, 1985.

[13] Gill, D., Michalakes, J., Dudhia, J., Skamarock, W., and Gopalakrishnan, S. Nesting in WRF 2.0. *Joint MM5/WRF Users Workshop, Boulder, Colorado, June 22-25* (2004).

[14] Haertel, P., and Johnson, R. The linear dynamics of squall line Mesohights and wake lows. *Journal of Atmospheric Sciences 57* (2000), 93–107.

[15] Hane, C. Extratropical squall lines and rainbands. *Mesoscale Meteorology and Forecasting, P. S. Ray., Ed., Americain Meteorology Society.* (1986), 359–389.

[16] Hong, S., and Pan, H. Nonlocal boundary layer vertical diffusion in a Medium-Range Forecast model. *Monthly Weather Review 124* (1996), 2322–2339.

[17] Houze, R. *Cloud dynamics.* International Geophysics Series, 1993.

[18] Janjic, Z. The step-mountain Eta Coordinate model: further developments of the convection, viscous sublayer and turbulence closure schemes. *Monthly Weather Revue 122* (1994), 927–945.

[19] Lafore, J., Stein, J., Asencio, N., Bougeault, P., Ducrocq, V., Duron, J., Fischer, C., Héreil, P., Mascart, P., Masson, V., Pinty, J., Redelsperger, J.L. Richard, E., and de Arellano J., V.-G. The Meso-NH Atmospheric Simulation System. Part I: adiabatic formulation and control simulations. Scientific objectives and experimental design. *Annales Geophysicae 16* (1997), 90–109.

[20] Mellor, G., and Yamada, T. A hierarchy of turbulence closure models for planetary boundary layers. *Journal of Atmospheric Sciences 31* (1974), 1791–1806.

[21] Monin, A., and Obukhov, A. Basic laws of turbulent mixing in the ground layer of the atmosphere. *Tr. Geofiz. Inst. Akad. Nauk SSSR 151* (1954), 163–187.

[22] Nuissier, O., Ducrocq, V., Ricard, D., Lebeaupin, C., and Anquetin, S. A numerical study of three catastrophic precipitating events over Southern France. Part I: Numerical framework and synoptic ingredients. *Quarterly Journal of the Royal Meteorological Society 134* (2008), 111–130.

[23] Pinty, J., and Jabouille, P. A mixed-phase cloud parameterization for use in a mesoscale non-hydrostatic model: Simulations of a squall line of orographic precipitation. *Preprints of Conf. on Cloud Physics, Everett, Washington, Americain Meteorological Society* (1998), 217–220.

[24] Ramis, C., Arus, J., and Lopez, J. Two cases of severe weather in Catalonia(Spain). A diagnostic study. *Meteorological Applications 6* (1999), 11–27.

[25] Ramis, C., Arus, J., Lopez, J., and Mestres, A. Two cases of severe weather in Catalonia(Spain). An observational study. *Meteorological Applications 4* (1997), 207–207.

[26] Ramis, C., Romero, R., and Homar, V. The severe thunderstorm of 4^{th} october 2007 in Mallorca: an observational study.

[27] Reisner, J., Rasmussen, R., and Bruintjes, R. Explicit forecasting of supercooled liquid water in winter storms using the MM5 mesoscale model. *Quarterly Journal of the Royal Meteorological Society 124B* (1998), 1071–1107.

[28] Romero, R., Doswell, C., and Riosalido, R. Observations and fine-grid simulations of a convective outbreak in northeastern Spain: importance of diurnal forcing and convective cold pools. *Monthly Weather Review 129* (2001), 2157–2182.

[29] Rotunno, R., and Klemp, J. On the rotation and propagation of simulated supercell thunderstorms. *Journal of Atmospheric Sciences 42* (1985), 271–292.

[30] Rotunno, R., Klemp, J., and Weismann, M. A theory for strong, long-lived squall line. *Journal of Atmospheric Sciences 45* (1988), 463–485.

[31] Stein, J., Richard, E., Lafore, J., Pinty, J., Asencio, N., and Cosma, S. High-resolution non-hydrostatic simulations of flash-flood episodes with grid-nesting and ice-phase parameterization. *Meteorology and Atmospheric Physics 72* (2000), 203–221.

[32] Tessendorf, S., and Trapp, R. On the climatological distribution of tornadoes within quasi-linear convective systems. *Preprints, 20th Conf. on Severe Local Storms, Orlando, FL, American Meteorological Society* (2000), 134–173.

[33] Trapp, R., and Weisman, M. Low-level mesovortices within squall lines and bow echoes. Part II: Their genesis and implications. *Monthly Weather Revue 131* (2003), 2804–2817.

[34] Wakimoto, R., Murphy, H., Davis, C., and Atkins, N. High winds generated by bow echoes. Part II: The relationship between the mesovortices and damaging straight-lines winds. *Monthly Weather Review 134* (2006), 2813–2829.

[35] Weisman, M., and Trapp, R. Low-level mesovortices within squall lines and bow echoes. Part I: Overview and dependence on environmental shear. *Monthly Weather Revue 131* (2003), 2779–2803.

[36] Wheatley, D., and Trapp, R. The effect of mesoscale heterogeneity on the genesis and structure of mesovortices within quasi-linear convective systems. *Monthly Weather Review 136* (2008), 4220–4241.

List of Figures

List of Tables